GROUND STATES OF TRITON AND ALPHA NUCLEI

BY

KUMBIRAI THEOTIMUS CHINYANGA

GROUND STATES OF TRITON AND ALPHA NUCLEI

by

KUMBIRAI THEOTIMUS CHINYANGA

submitted in accordance with the requirements
for the degree of

MASTER OF SCIENCE

in the subject

PHYSICS

at the

UNIVERSITY OF SOUTH AFRICA

SUPERVISOR : PROFESSOR G. J. RAMPHO

NOVEMBER 2022

Declaration

Student Name : K. T. Chinyanga

Student No. : 4587 1191

I declare that **" GROUND STATES OF TRITON AND ALPHA NUCLEI"** is my own work and that all the sources that I have used or quoted have been indicated and acknowledged by means of complete references.

SIGNATURE DATE

Acknowledgments

I would like to thank Prof G. J. Rampho for his expert guidance, patience and inspiration throughout this research.

I would like to thank my friends and fellow students Mr M. Ramantswana and Mr E. C. Ojukwu for encouragement and support.

I would like to thank my three children Ropafadzo, Rindayi and Anemutsa for prayers and inspiration.

I would like to thank my wife, Mrs. M. Chinyanga, for her encouragement and support.

Summary

The few-body integrodifferential equations are approximations to the few-body Schrödinger equation in hyperspherical coordinates. The few-body integrodifferential equations for identical particles reduce to a single integrodifferential equation in two variables only. The structure of the integrodifferential equation does not dependent of the number of particles in the system. The integrodifferential equation has previously been solved using the adiabatic approximation method, the projection method and the perturbation method. In this dissertation we solve the few-body integrodifferential equations directly using the Lagrange mesh method. We apply the equations to Triton and alpha nuclei which are three-body and four-body systems, respectively. We treat the nucleons as interacting through spin-dependent nucleon-nucleon potentials. The few-body integrodifferential equations develop into a system coupled integrodifferential equations in the case of spin-dependent potentials. All our results are compared to those found in literature.

Keywords: Eigenvalue Problem; Faddeev equations; Few-body Systems; Ground-state Energy; Hyperspherical Harmonics; Hypercentral Potential; Integrodifferential Equations Approach; Potential Harmonics; Spin-dependent potential; Symmetric states

Contents

List of Tables

List of Figures

Chapter 1

Introduction

The battle to understand the universe rages on. Among the fundamental questions crucial to the better understanding of the universe has been the need for a theoretical framework that successfully explains the structure, properties and dynamics of molecular, atomic, nuclear and composite particle systems. The advent of a quantum mechanical framework brought much relief to the perplexities and ideological challenges of interested researchers.

A quantum mechanical framework has been the only vehicle through which the structure, properties and dynamics of molecular, atomic and nuclear systems have been successfully accounted for [1, 2]. The investigation of these systems involves solving Schrödinger or Schrödinger-like equations [3]. Challenges within the quantum mechanical model have persisted because analytical solutions to the Schrödinger equation are only available for a few idealised cases [4]. Of note is the few-body problem. With similarity to the classical few-body problem, which has only analytical solutions up to only two bodies [5], the few-body quantum-mechanical problem has only few practical analytical solutions. These include the hydrogen atom, the hydrogen molecular ion and the helium atom [1, 6].

The solution of the few- and many-body Schrödinger equation is often used in theoretical studies of quantum mechanical systems, like nuclear, atomic and molecular systems. Properties of these systems, such as charge distributions, root-mean-square radii, binding energies, energy levels, magnetic moments, among others, can be extracted from

the solution of the Schrödinger equation for the system [4]. Theoretical studies of these physical systems need accurate mathematical descriptions of the interactions in these systems [4]. Challenges in solving the few-body Schrödinger equation stem from two main problems. The equation results in a huge number of degrees of freedom, and some underlying interactions may not be fully understood as is the case in nuclear systems. This implies that we have to resort to some assumptions and approximations in order to construct theoretical models for numerical treatments so as to solve the few-body Schrödinger equation [4]. These theoretical models are difficult to construct [4, 7]. The success of these models depends mainly on being able to successfully account for experimental results [8].

Among the practical three- and four-body systems that have been widely investigated are the Triton and alpha particles. They have been widely investigated because their experimental and theoretical data is widely available for comparison. They have become a testing ground for the applicability and correctness of quantum mechanical models. It should also be pointed out that they are building blocks of some many-body systems. Therefore, a good understanding of these systems will lead to a better understanding of the many-body systems they build. They have been investigated using the Faddeev and the Faddeev-Yakubovsky methods [9, 10], the hyperspherical harmonic expansion method (HHEM) [11, 12], The Faddeev approach, the integrodifferential approach (IDEA). [13, 14, 15, 16, 17, 18].

The Faddeev formalism was introduced in the early 1960s by Faddeev [19]. It was most popular in solving scattering problems [18, 19]. The Faaddeev formalism assumes that particles interact only via two-body potentials. Therefore the total potential is taken as a sum of these two-body potentials. The wave function is thus taken as a sum of two-body amplitudes. This formalism managed to give exact solutions to the Schrödinger equation for three-body systems. Yakubovsky extended the Faddeev formalism to four

bodies [10], and also gave exact results. However, for more than four bodies the Faddeev formalism becomes too complicated to solve both analytically and numerically. Both the Faddeev and Faddeev-Yakubovsky equations can be formulated in configuration and momentum space. In configuration space, using Jacobi coordinates, they result in integrodifferential equations whereas in momentum space, they result in integral equations. The Faddeev differential equations have been investigated by Gignoux, Carbonell and Merkriev [20, 21] and the Faddeev-Yakubovsky differential equations have been investigated by Yakovlev and Yakubovsky [10, 21]. The Alt-Grasberger-Sandhas equations are formulated in the momentum space and have been used widely in solving problems of three and four-body scattering and break-up reactions [22, 23].

The HHEM was introduced in 1935 [24] and were revisited in the 1960s [25, 26, 27], and is currently one of the state-of-the-art methods in few-body physics [28]. The HHEM reduces the N-body Schrödinger equation to system of coupled ordinary differential equations in a single variable. The advantages of the HHEM is that analytical expressions of the matrix elements are available in most cases and the convergence properties of hyperspherical harmonics expansion are known [29]. The disadvantages of the HHEM is that it has slow convergence. Its complexity also increases as the number of constituent particles increases [13, 14]. Hyperspherical harmonics have been used to solve three- and four-body systems such as helium and lithium atoms [30, 31, 32], nuclear systems such as Triton and α particles [28, 33] and hadronic calculations [34].

As indicated earlier, the use of hyperspherical harmonics to solve the Schrödinger equation results in an infinite number of coupled differential equations. The number of these equations has to be truncated for numerical implementation. Convergence of the hyperspherical harmonics expansion is usually slow due to the large number of independent harmonics of the grand orbital quantum number, since each equation is related to one hyperspherical harmonic. This leads to a very large number of coupled equations that

has to be solved, thus, resulting in slow convergence. To solve this problem, the use of Potential harmonics, which are a subset of hyperspherical harmonics was introduced [35, 36]. This significantly reduces the number of coupled equations that have to be solved. However, the number of equations to be solved increases significantly when the number of particles increases even when Potential Harmonics are used. This motivated for the conception of few-body integrodifferential equations approach [13, 14].

To deal with the problem of the slow convergence of hyperspherical harmonics and Potential harmonics, the Schrödinger equation in hyperspherical coordinates is expressed as a set of coupled integrodifferential equations using Faddeev formalism into. These few-body integrodifferential equations generalises the three-body Faddeev equations to treat many-body systems, but retains the three-body like structure. However, only two-body correlations are taken into account in this approach [13]. Fabre et al, showed that under certain simplifications, for three-body systems, these integrodifferential equations reduce to the Faddeev equations. These integrodifferential equations have been applied to four-body systems, to sixteen-fermion system interacting via a Wigner-type potential [14]. The approach has been used to study nucleon systems with more realistic interaction potentials [13, 37, 38]. It has also been applied to Bose-Einstein condensates [18]. In all these applications, it has been found that the integrodifferential equations approach, produces results that are similar to those reported in literature. The integrodifferential equations approach have been found to be extremely convenient because, unlike the other indicated competing methods, its complexity does not change as the number of constituents in the system increases [13, 14].

So far the integrodifferential equation has been solved by the adiabatic approximation method [13, 40, 41, 42] that decouples the integrodifferential equations into single-variable radial and angular equations. The perturbation method [43, 44] has also been used to solve the integrodifferential equations iteratively from the unperturbed state.

On the other hand, the projection method solves the integrodifferential equation by expanding its solution in a complete set of Jacobi polynomials leading to a system of second order coupled differential equations [40]. All these solution methods have shortcomings that have been indicated, hence the need to investigate the solution of these equations using other methods. Rampho [45] regularised the integrodifferential equations so that they have boundary conditions in the hyperadial and angular domains. The numerical solution of the regularised integrodifferential equations using the Lagrange-mesh method has been shown to converge rapidly. However, these equations and the solution method have not yet been investigated in the presence of spin-dependent potentials.

In this dissertation we solve the regularised integrodifferential equations for the Triton and alpha particle with spin-dependent potentials using the Lagrange-mesh method. The Lagrange-mesh method has been used to solve many quantum mechanical problems with very high accuracy [3]. It has been used to solve the Schrödinger equation in momentum space, whose non-local kernels are very similar to those of the integrodifferential equation [46, 47]. This method has also been used to solve the one-dimensional Schrödinger equation, the time-dependent Schrödinger equation, scattering problems, Hartree-Fock calculations, the Dirac equation among many more problems [3]. The successes of the Lagrange-mesh method in all these problems and its notable high accuracy in most of these cases is the motivation behind our implementation of this method in solving the coupled integrodifferential equations resulting from the presence of spin-dependent potentials.

This dissertation is organised into five charpters. In Chapter 1, we have analysed the literature on the problem we wish to solve and the solution method more suitable to this problem. In Chapter 2, we discuss key features of the integrodifferential equations approach. In Chapter 3, we outline key features of the Lagrange-mesh method and

how it is used to solve the integrodifferential equations. In Chapter 4, we present and discuss results for the Triton and alpha nuclei involving spin-dependent potentials. In Chapter 5, we summarize conclusions.

Chapter 2

Integrodifferential Equations Approach

2.1 Many-body coordinate systems

We construct coordinates for a system of A number of particles. We consider the particles to each have mass m_i and position vector $\boldsymbol{x}_i$, $(i = 1, 2, ..., A)$ and interacting through two-body potentials. The Schrödinger equation for this system is given by [47]

$$\left[-\sum_{i}^{A} \frac{\hbar^2}{2m_i} \nabla_i^2 + \sum_{ij}^{A} V(\boldsymbol{r}_{ij}) - E \right] \Psi(\boldsymbol{x}) = 0 \tag{2.1}$$

where $\boldsymbol{x} \equiv \{ \boldsymbol{x}_1, \boldsymbol{x}_2 .... \boldsymbol{x}_A)$, E is the energy, $\Psi(\boldsymbol{x} \}$ the wavefunction of the system and $V(\boldsymbol{r}_{ij})$ the two-body potentials with $\boldsymbol{r}_{ij} = \boldsymbol{x}_i - \boldsymbol{x}_j$. As can be seen, the Schrödinger equation (2.1) is multi-dimensional and has a large number of variables. In constructing the solutions to the many-body Schrödinger equation (2.1), only the internal motions of the particles are relevant. Wavefunctions which describe these internal motions must be translationally and rotationally invariant. In order to achieve this the Jacobi coordinate system is constructed.

Jacobi coordinates enable the motion of the center-of-mass and internal motion of the system to be readily separated. For the A-body system, we define $N = A - 1$ Jacobi vectors [13, 48]

$$\xi_N = \left[\frac{2Am_1m_2}{M(m_1 + m_2)} \right]^{1/2} (\boldsymbol{x}_2 - \boldsymbol{x}_1)$$

$$
\begin{aligned}
\xi_{N-1} &= \left[\frac{2A(m_1+m_2)m_3}{M(m_1+m_2+m_3)}\right]^{1/2}\left(\boldsymbol{x}_3 - \frac{m_1\boldsymbol{x}_1+m_2\boldsymbol{x}_2}{m_1+m_2}\right)\\
&\vdots\\
\xi_{N-i+1} &= \left[\frac{2A(\sum_{j=1}^{i} m_j)m_{j+1}}{M(\sum_{j=1}^{i} m_j)}\right]^{1/2}\left(\boldsymbol{x}_{i+1} - \frac{\sum_{j=1}^{i} m_i\boldsymbol{x}_i}{\sum_{j=1}^{i} m_j}\right)\\
&\vdots\\
\xi_1 &= \left[\frac{2A(M-m_A)m_A}{M^2}\right]^{1/2}\left(\boldsymbol{x}_A - \frac{\sum_{j=1}^{A-1} m_j\boldsymbol{x}_j}{M-m_A}\right) \qquad (2.2)
\end{aligned}
$$

which enable the elimination of the center-of-mass. The center-of-mass $\boldsymbol{X}$ and total mass M of the system are given by

$$
\boldsymbol{X} = \frac{1}{M}\sum_{j=1}^{A} m_j\boldsymbol{x}_j \qquad \text{and} \qquad M = \sum_{j=1}^{A} m_j\,, \qquad (2.3)
$$

respectively. When the particles are identical, with equal mass, these vectors reduce to [13]

$$
\begin{aligned}
\xi_N &= \boldsymbol{x}_1 - \boldsymbol{x}_2 = \boldsymbol{r}_{12}\\
\xi_{N-1} &= \sqrt{3}(\boldsymbol{x}_3 - \boldsymbol{X}_3)\\
&\vdots\\
\xi_{N-1+i} &= \sqrt{\frac{2(i+1)}{i}}(\boldsymbol{x}_{i+1} - \boldsymbol{X}_{i+1}) = \sqrt{\frac{2i}{i+1}}(\boldsymbol{x}_{i+1} - \boldsymbol{X}_{i+1})\\
&\vdots\\
\xi_1 &= \sqrt{\frac{2A}{A-1}}(\boldsymbol{x}_A - \boldsymbol{X}), \qquad X_i = \frac{1}{i}\sum_{j=1}^{i}\boldsymbol{x}_j, \qquad \boldsymbol{X}_A = \boldsymbol{X}\,. \qquad (2.4)
\end{aligned}
$$

We have give a more general description of the Jacobi vectors than used in this work. In this dissertation we only require Jacobi vectors for three-body ($A = 3$) and four-body ($A = 4$) systems. The given Jacobi vectors are now used to construct hyperspherical coordinates and corresponding Hamiltonian for the system.

In the Jacobi vectors, the total kinetic energy operator for the system can be expressed

in the form [49, 50]

$$-\frac{\hbar^2}{2}\sum_{i=1}^{A}\frac{1}{m_i}\nabla^2 = -\sum_{j=1}^{A}\frac{\hbar^2 A}{M}\nabla_{\xi_j}^2 - \frac{\hbar^2}{2M}\nabla_{\boldsymbol{X}}^2 \tag{2.5}$$

$$= T_{internal} + T_{cm} \tag{2.6}$$

where $T_{internal}$ and T_{cm} are the kinetic energy operators for the internal and center-of-mass motion, respectively. Solutions to the Laplace operator whose structure is given by equation (2.6) can be separated into products of a function that depends on the center-of-mass and a function that depends on translationally invariant internal coordinates only. The separation of the center-of-mass from the internal motion is based on the assumption that only hyperspherical harmonics of degree zero in the center-of-mass are dominant [24, 35].

From the Jacobi vectors, we construct hyperspherical coordinates for the A-body system. Such coordinates consist of a hyperradius r and $3N-4$ angular coordinates. The hyperradius is defined using the inter-particle coordinates $\boldsymbol{r}_{ij} = \boldsymbol{x}_i - \boldsymbol{x}_j$ as [51]

$$r = \left[\frac{2A}{M^2}\sum_{i<j<A} m_i m_j (\boldsymbol{x}_i - \boldsymbol{x}_j)^2\right]^{\frac{1}{2}} = \left[\frac{2A}{M^2}\sum_{i<j<A} m_i m_j (\boldsymbol{r}_{ij})^2\right]^{\frac{1}{2}} = \left[\sum_{i=1}^{N}\xi_i^2\right]^{\frac{1}{2}} \tag{2.7}$$

which reduce to [13]

$$r = \left[2\sum_{i=1}^{A}(\boldsymbol{x}_i - \boldsymbol{x}_j)^2\right]^{\frac{1}{2}} = \left[2\sum_{i=1}^{A}(\boldsymbol{x}_i - \boldsymbol{X})^2\right]^{\frac{1}{2}} = \left[\frac{2}{A}\sum_{i<j<A} r_{ij}^2\right]^{\frac{1}{2}} \tag{2.8}$$

for identical particles. There are several ways of choosing the angular set

$$\Omega(\omega_1, \omega_2, \ldots, \omega_N; \phi_2, \phi_2, \ldots, \phi_N)$$

describing the other $3A-4$ degrees of freedom. Vilenkin Kuznetsov and Smorodinsky [52] gave a comprehensive description.

The Zernike and Brinkman provide a simpler description of the set Ω which consists of spherical coordinates $\omega_i = (\theta_i, \varphi_i)$ for each Jacobi vector $\boldsymbol{\xi}_i$ and the hyperspherical

angles $\phi_i (i = 2, 3, ..., N)$ are defined by [50, 51]

$$\tan\phi_i = \frac{1}{\xi_i}\sqrt{\sum_{j=1}^{i-1}\xi_j} \tag{2.9}$$

and are related to the magnitudes of the Jacobi vectors by

$$\begin{aligned} \xi_N &= r\cos\phi_N \\ \xi_{N-1} &= r\sin\phi_N\cos\phi_{N-1} \\ \xi_i &= r\sin\phi_N\ \ldots\ \sin\phi_{i+1}\cos\phi_i \qquad (\phi_1 = 0)\,. \end{aligned} \tag{2.10}$$

A surface element on the $(D-3)$-dimensional hypersphere is defined by [13, 48]

$$d\Omega = d\omega_1 \prod_{j=1}^{N} d\omega_j (\sin\phi_j)^{3j-4}\cos^2\phi_j\, d\phi_j \tag{2.11}$$

recalling that $\phi_1 = 0$. In particular, for $j = N$, we have

$$d\Omega = (\sin\phi)^{D-4}\cos^2\phi\, d\phi\, d\omega\, d\Omega_{N-1} \tag{2.12}$$

where $\phi = \phi_N$, $\omega = \omega_N$.

For convenience, we now define a transformation variable z_j as

$$z_j = \cos 2\phi_j \tag{2.13}$$

and $z_j \in [-1, +1]$. For $j = N$, we have $z = \cos 2\phi_N$. In the new variable z, the inter-particle separation vector is given by

$$r_{ij} = r\cos\phi_N = r\sqrt{\frac{1+z}{2}}\,. \tag{2.14}$$

On the other hand, in the variable z we get

$$d\Omega = 2^{-(\alpha+\beta+1)}(1-z)^{\alpha}(1+z)^{\beta}\, dz\, d\omega\, d\Omega_{N-1} \tag{2.15}$$

where $\alpha = (3\,A - 8)/2$ and $\beta = 1/2$. This surface element can be written in compact form as

$$d\Omega = 2^{-(\alpha+\beta+1)}\, w(z)\, dz\, d\omega\, d\Omega_{N-1} \tag{2.16}$$

where $w(z) = (1-z)^{\alpha}(1+z)^{\beta}$. The volume element in the $D-$dimensional space is constructed from the surface element as

$$d^D\xi = r^{D-1}\, dr\, d\Omega \tag{2.17}$$

where $D = 3(A-1)$. In what follows, the hyperspherical coordinates are used to construct hyperspherical harmonics for the A-body system.

2.2 Potential Harmonics

The integrodifferential equations approach is derived using Potential Harmonics which are a subset of the hyperspherical harmonics. We, therefore, need to give a brief background of hyperspherical harmonics. To this end, we introduce harmonic polynomials $H_{[L]}(\xi)$ $(\xi = \xi_1, \xi_2, \ldots \xi_N)$ where $[L]$ represents the $3N-1$ quantum numbers. These are homogeneous polynomials of degree L defined by the Laplace equation [35, 53]

$$\sum_{j=1}^{N} \nabla^2_{\xi_j} H_{[L]}(\xi) = 0\,, \tag{2.18}$$

and form a complete orthogonal set of polynomials. Therefore, any continuous function can be approximated with a superposition of these polynomials by [38]

$$\Psi(\boldsymbol{x}) = \sum_{[L]=0}^{\infty} H_{[L]}(\hat{\boldsymbol{x}})\, \phi_{[L]}(r) \tag{2.19}$$

where $H_{[L]}(\hat{\boldsymbol{x}})$ is a harmonic polynomial in all the variables $\boldsymbol{x}$ characterised by $3N-1$ quantum numbers $[L]$. The harmonic polynomials over the unit hypersphere are called hyperspherical harmonics $Y_{[L]}(\Omega)$ of order L. They satisfy the orthogonality condition [13]

$$\int Y^*_{[L]}(\Omega)\, Y_{[L]}(\Omega)\, d\Omega = \delta_{[L],[L']} \tag{2.20}$$

where $\delta_{[L],[L']}$ is the Kronecker delta, on the surface of a unit hypersphere. These hyperspherical harmonics are related to the harmonic polynomials as

$$Y_{[L]}(\Omega) = r^{-L}\, H_{[L]}(\boldsymbol{\xi}) \tag{2.21}$$

where $\boldsymbol{\xi} = \{\, \xi_1, \xi_2, \ldots, \xi_N \,\}$.

The hyperspherical harmonics $Y_{[L]}(\Omega)$ are defined by [13, 48]

$$Y_{[L]}(\Omega) = Y_{l_1}^{m_1}(\omega_1) \prod_{j=2}^{N} Y_{l_j}^{m_j}(\omega_j)\, {}^{(j)}P_{[L_j]}^{l_j, Lj-1}(\phi) \tag{2.22}$$

where $Y_{l_j}^{m_j}(\omega_j)$ are spherical harmonics,

$${}^{(j)}P_{[L_j]}^{l_j, L_{j-1}}(\phi) = N_{L_j, l_j}^2 (1 - z_j)^{L_{(j-1)}/2} P_{n_j}^{\nu_{j-1}, l_j + 1/2}(\phi) \tag{2.23}$$

and $P_{n_j}^{\nu_{j-1}, l_j+1/2}(\phi)$ are Jacobi polynomials with normalization coefficient

$$N_{L_j, l_j}^2 = \frac{2^{1-(L_{j-1}+l_j)}\, \nu_j\, n_j\, \Gamma(\nu_j - n_j)}{\Gamma(\nu_j - n_j - l_j - \frac{1}{2}) \Gamma(n_j + l_j + \frac{3}{2})}\,. \tag{2.24}$$

In these expressions, the notation $\nu_j = L_j + \frac{3j}{2} - 1$, $L_j = l_1 + \sum_{k=2}^{j} (\, 2\, n_k + l_k \,)$ are used where $L = L_N = \sum_{i=1}^{N} (\, 2\, n_i + l_i \,)$ is the grand orbital angular momentum quantum number with l_i and n_i as intermediate orbital quantum numbers.

The Laplacian in hyperspherical coordinates has the form [51]

$$\nabla^2 \equiv \sum_{i=1}^{N} \nabla_{\xi_i}^2 = \frac{\partial^2}{\partial r^2} + \frac{3A - 4}{r} \frac{\partial}{\partial r} + \frac{\hat{L}^2(\Omega)}{r^2} \tag{2.25}$$

where $\hat{L}^2(\Omega)$ is the grand orbital angular momentum operator which is generated from the recurrence relation

$$\hat{L}^2(\Omega) = \frac{4}{w(z)} \frac{\partial}{\partial z} (1 - z^2)\, w(z) \frac{\partial}{\partial z} + \frac{2\, \hat{l}^2(\omega)}{1 + z} + \frac{2\, \hat{L}^2(\Omega_{N-1})}{1 - z} \tag{2.26}$$

where $\hat{L}^2(\Omega) \equiv \hat{L}^2(\Omega_N)$ and $\hat{L}^2(\Omega_1) = \hat{l}^2(\omega_1)$. The operators $\hat{l}^2(\omega_i)$ $(i = 1, ..., N)$ satisfy the eigenvalue equations

$$\left[\, \hat{l}^2(\omega_i) + l_i(l_i + 1) \,\right] Y_{l_i}^{m_i}(\omega_i) = 0 \tag{2.27}$$

where $Y_l^m(\omega)$ are the spherical harmonics. The eigenfunctions $Y_{[L]}(\Omega)$ of the grand orbital angular momentum operator $\hat{L}^2(\Omega)$ are solutions to the eigenvalue equation

$$\left[\, \hat{L}^2(\Omega) + L(L + D - 2) \,\right] Y_{[L]}(\Omega) = 0\,. \tag{2.28}$$

where D is the dimensionality of the space. In practical applications, like many-body quantum systems where two-body correlations are dominant, the number of hyperspherical harmonics basis can be reduced to a subset called the potential harmonic basis.

A set of potential harmonic basis $\mathcal{P}^{l,m}_{2K+l}(\Omega_{ij})$ is defined as the set of hyperspherical harmonics associated with an interaction potential model $V(\boldsymbol{r}_{ij})$ [35, 36]. This basis is also complete and can be used to approximate any function of $\boldsymbol{r}_{ij}$. For a pair of interacting particles (ij) in a state with orbital angular momentum l while all the other pairs are in an s-state, the potential basis satisfy the relation [35, 36]

$$\hat{L}^2(\Omega_{N-1})\,\mathcal{P}^{l,m}_{2K+l}(\Omega_{ij}) = 0 \tag{2.29}$$

where $K = 0,\, 1,\, 2, \ldots$. In this case, the basis has the form [35, 36]

$$\mathcal{P}^{l,m}_{2K+l}(\Omega_{ij}) = N_{K,l}\, Y^m_l(\omega_{ij})\, \left(\frac{r_{ij}}{r}\right)^l\, P^{\alpha,\beta}_K(2r^2_{ij}/r^2 - 1) \tag{2.30}$$

where $\beta = l + 1/2$ and $N_{k,l}$ is the normalisation constant. They also obey the orthogonality condition

$$\int d\Omega\, \mathcal{P}^{l,m*}_{2K+l}(\Omega_{ij})\, \mathcal{P}^{l',m'}_{2K'+l'}(\Omega_{ij}) = \delta_{KK'}\, \delta_{ll'}\, \delta_{mm'}\,. \tag{2.31}$$

Two-body potentials in S-state can be expanded in terms of potential harmonics as [14, 35, 54]

$$V(r_{ij}) = \sum_{K=0}^{\infty} \mathcal{P}^{00}_{2K}(\Omega_{ij})\, V_K(r) \tag{2.32}$$

where the expansion coefficients $V_K(r)$ are called potential multipoles. These multipoles are given by [35, 50, 55]

$$\begin{aligned} V_K(r) &= \int_0^{2\pi} V(r\cos\phi)\, \mathcal{P}^{00}_{2K}(\Omega_{ij})\, d\Omega & (2.33)\\ &= [N^{\alpha,\beta}_K]^{-1} \int_{-1}^{1} V(r\sqrt{(1+z)/2})\, P^{\alpha,\beta}_K(z)\, w(z)\, dz\,. & (2.34) \end{aligned}$$

The coefficients $V_K(r)$ are also referred to as the hypercentral potentials. It is defined as the potential that operate on the $l \neq 0$ orbitals of the two-body potential [56]. The

first term $V_0(r)$, called the zeroth order potential multipole [56, 57] of the hypercentral potential contains the most important part of the hypercentral potential [14].

2.3 Few-body integrodifferential equations

When two-body correlations are dominant in a many-body system, then the many-body Schrödinger equation can be expressed in the form $\Psi(\boldsymbol{x}) = \sum_{i<j<A} \phi_{ij}(\boldsymbol{x})$ where $\phi_{ij}(\boldsymbol{x})$ are two-body amplitudes. Then, the Schrödinger equation (2.1) is decomposed into $\frac{1}{2}A(A-1)$ coupled equations [48]

$$[\,T - E\,]\;\phi_{ij}(\boldsymbol{x}) = -V(r_{ij})\,\Psi(\boldsymbol{x}) \tag{2.35}$$

where T is the internal kinetic energy operator of the system. In terms of the hyperspherical harmonics discussed earlier, the two-body amplitudes have the form [38]

$$\phi_{ij}(\boldsymbol{x}) = H_{[L]}(\boldsymbol{x})\,G(\boldsymbol{r}_{ij}, r) \tag{2.36}$$

where $G(\boldsymbol{r}_{ij}, r)$ depends only on $\boldsymbol{r}_{ij}$ and r. Then, the equations (2.35) are written in the form [48]

$$[\,T - E\,]\;H_{[L]}(\boldsymbol{x})\,G(\boldsymbol{r}_{ij}, r) = -V(r_{ij})\,H_{[L]}(\boldsymbol{x}) \sum_{k<l\leq A} G(\boldsymbol{r}_{ij}, r)\,. \tag{2.37}$$

However, for systems in S-state, states with $L = 0$ which are considered in this work, the harmonic polynomials is given by

$$H_{[0]}(\boldsymbol{x}) = \left[\frac{\Gamma(D/2)}{2\pi^{(D)/2}}\right]^{1/2} = \text{constant}\,. \tag{2.38}$$

In this case, equations (2.37) reduce to

$$[\,T - E\,]\;G(\boldsymbol{r}_{ij}, r) = -V(r_{ij}) \sum_{k<l\leq A} G(\boldsymbol{r}_{ij}, r) \tag{2.39}$$

for systems in S-state.

The equations (2.39) need to be modified to account for the effects of higher partial waves of the two-body potential. Adding the zeroth potential multipole accounts for the effects of higher orbital angular momentum [13, 14, 35]. Therefore, the equations are modified by adding $V_0(r)$ to (2.39) to obtain [48]

$$\left[T + \frac{1}{2} A\,(\,A-1\,)\,V_0(r) - E \right] G(\boldsymbol{r}_{ij}, r) = -\,[\,V(r_{ij}) - V_0(r)\,] \sum_{k<l\leq A} G(\boldsymbol{r}_{ij}, r) \quad (2.40)$$

where $V(r_{ij}) - V_0(r)$ is called the residual interaction. Here, the hypercentral potential is calculated by [45]

$$V_0(r) = \frac{1}{\pi} \int_{-1}^{+1} V(r,z)\,\sqrt{1-z^2}\,dz \quad (2.41)$$

for both 3-body and 4-body systems. To account for boundary conditions, the amplitudes $G(r_{ij}, r)$ are transformed by [45]

$$G(r_{ij}, r) = \frac{F(z,r)}{\sqrt{r^{(D-1)}\,w(z)}} \quad (2.42)$$

where $F(z,r)$ are the reduced two-body amplitudes. Expanding the amplitudes $F(r_{ij}, r)$ in terms of potential harmonics and projecting on the r_{ij} space yields the coupled integrodifferential equations [48]

$$\begin{aligned} &\left\{ \frac{\hbar^2}{m} \left[-\frac{\partial^2}{\partial r^2} + \frac{\mathcal{L}_0(\mathcal{L}_0+1)}{r^2} - \frac{4}{r^2}\,\frac{1}{w(z)}\,\frac{\partial}{\partial z}(1-z^2)\,w(z)\,\frac{\partial}{\partial z} \right] + N_p\,V_0(r) - E \right\} F(z,r) \\ &= -\big[\,V(r,z) - V_0(r)\,\big] \left[F(z,r) + \int_{-1}^{+1} f(z,z')\,F(z',r)\,dz' \right] \end{aligned} \quad (2.43)$$

where $N_p = A(A-1)/2$, $V(r,z) = V(r\sqrt{(1+z)/2})$, $\mathcal{L}_0 = 3A/2 - 3$ and $f(z,z')$ is the projection kernel. The factor in the curly brackets on the right-hand-side of (2.43) represents the total wavefunction of the system.

The projection kernel represents kinematical rotations between different Jacobi orientations of the system. The projection kernel is defined in terms of Jacobi polynomials as [14]

$$f(z,z') = w(z') \sum_K \frac{(f_K^2 - 1)\,P_K^{\alpha,\beta}(z)\,P_K^{\alpha,\beta}(z')}{h_K^{\alpha,\beta}} \quad (2.44)$$

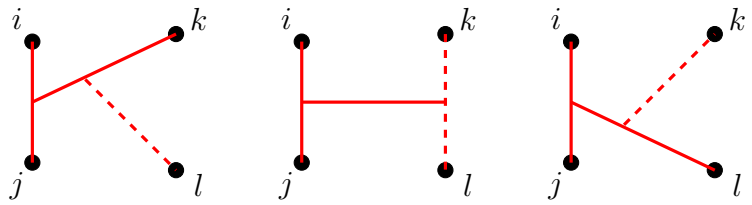

Figure 2.1: Jacobi partitions, in a four-body system, for the primary interacting pair $\{ij\}$.

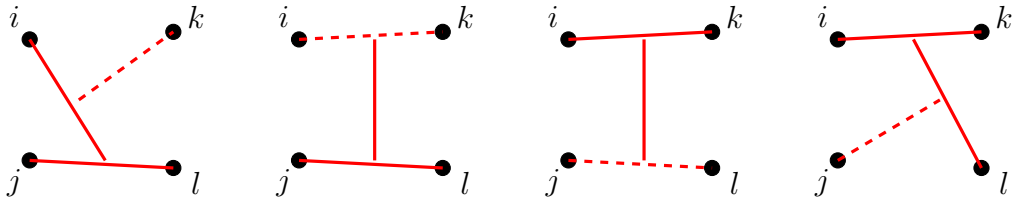

Figure 2.2: Jacobi partitions, in a four-body system, for other interacting pairs of particles, $\{ik\}$ and $\{jl\}$, that are connected to the pair $\{ij\}$.

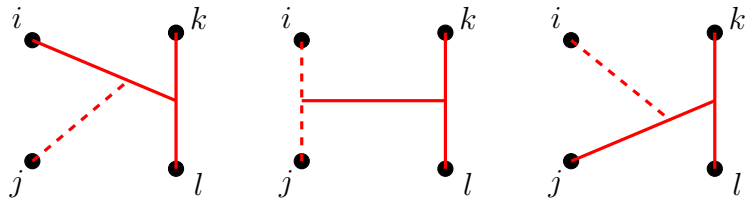

Figure 2.3: Jacobi partitions, in a four-body system, for other interacting pairs of particles, $\{kl\}$, that are not connected to the pair $\{ij\}$.

where

$$f_K^2 = 1 + \frac{[2(A-2)\,P_K^{\alpha,\beta}(-\frac{1}{2}) + \frac{(A-2)(A-3)}{2}\,P_K^{\alpha,\beta}(-1)]}{P_K(1)}\,. \tag{2.45}$$

This kernel is usually expressed in the form

$$f(z,z') = 2(A-2)\, f(z,z',-\frac{1}{2}) + \frac{(A-2)(A-3)}{2}\, f(z,z',-1) \tag{2.46}$$

where the first term refers to $2(A-2)$ pairs connected to the interacting pair $\{ij\}$, for which $\varphi_N = 2\pi/3$, while the last term refers to the $(A-2)(A-3)/2$ pairs not connected to the interacting pair $\{ij\}$, for which $\varphi = \pi/2$. Illustrations of Jacobi partitions for the interacting pair $\{ij\}$ are shown in Figure 2.1, for pair connected to the interacting pair are shown in Figure 2.2, for pair not connected to the interacting pair are shown in Figure 2.3. The illustrations represent kinematical rotations or permutations of particles in the system.

As indicated earlier, adding the zeroth ($K = 0$) hypercentral potential multipole to the coupled integrodifferential equations accounts for the effects of higher orbital angular momentum. However, spurious amplitudes are accounted for by subtracting the first-order ($K = 1$) potential multipole. Spurious amplitudes are amplitudes which are not physical, and arise when the amplitudes $F(\boldsymbol{r}_{ij}, r)$ are expanded using the $\mathcal{P}^{00}_{2K}(\Omega_{ij})$. Only effects of higher partial waves are considered in this work.

2.4 Spin-dependent potentials

Nucleons have a number of degrees-of-freedom, such as position, spin, isospin, parity and charge. Amplitudes for nucleons must depend on these degrees-of-freedom. We represent spin and isospin dependent two-body amplitudes as $\phi_{ij}(\boldsymbol{x}, s, t)$ where s (t) is the relative spin (isospin) of the pair $\{ij\}$. Consideration of spin and isospin in the two-body amplitudes introduces symmetry requirements in the wavefunction. We use the symbol A (S) to represent spin-isospin combinations that are totally antisymmetric (symmetric) and A'_{ij} (S'_{ij}) when antisymmetric (symmetric) with exchange of nucleons i and j only. The latter are referred to as mixed-antisymmetric (mixed-symmetric). The construction of the two-body amplitudes with spin and isospin is quite complicated

and the details are summarized [38]. The spin-dependent two-body amplitudes for even parity states, for central interactions, have the form [38]

$$\phi^{+}_{ij}(\boldsymbol{x},s,t) = \phi^{S}_{ij}(\boldsymbol{x},s,t)\,|\,A\,\rangle + \phi^{S'}_{ij}(\boldsymbol{x},s,t)\,|\,A'_{ij}\,\rangle \tag{2.47}$$

where completely symmetric and symmetric spin-isospin states are neglected. In general, the amplitudes have even (+) and odd (-) parity components where the parity of spacial components are opposite that of spin-isospin components.

The total wavefunction of the system is given by $\Psi(\boldsymbol{x},S,T) = \sum_{ij}\phi^{+}_{ij}(\boldsymbol{x},s,t)$ where S and T are the spin and isospin, respectively, of the system. The projection of the total wavefunction on the $\boldsymbol{r}_{ij}$ space require the rotation of spin-isospin states [38]

$$\begin{bmatrix} |\,A'_{ki}\,\rangle \\ |\,A'_{jk}\,\rangle \end{bmatrix} = \begin{bmatrix} -\frac{1}{2} & +\frac{\sqrt{3}}{2} \\ -\frac{1}{2} & -\frac{\sqrt{3}}{2} \end{bmatrix} \begin{bmatrix} |\,A'_{ij}\,\rangle \\ |\,S'_{ij}\,\rangle \end{bmatrix} \tag{2.48}$$

for three-body and four-body systems, with $|\,A'_{kl}\,\rangle = |\,A'_{ij}\,\rangle$ and $|\,S'_{kl}\,\rangle = |\,S'_{ij}\,\rangle$ for four-body systems. The projection of the total wavefunction leads to [38]

$$\langle \boldsymbol{r}_{ij}\,|\,\Psi(\boldsymbol{x})\rangle = Y^{0}_{0}(\omega_{ij})\,[\,\Pi^{S}(z,r)\,|\,A\,\rangle + \Pi^{S'}(z,r)\,|\,A'_{ij}\,\rangle\,] \tag{2.49}$$

where the spatial components are given by

$$\Pi^{\kappa}(z,r) = F^{\kappa}(z,r) + \int_{-1}^{+1} f_{\kappa}(z,z',-1)\,F^{\kappa}(z',r)\,dz' \tag{2.50}$$

with $\kappa = S, S'$. The associated project kernels have the form

$$f_{S}(z,z') = (A-2)\left[\frac{1}{2}(A-3)\,f(z,z',-1) + 2\,f(z,z',-\frac{1}{2})\right] \tag{2.51}$$

$$f_{S'}(z,z') = (A-2)\left[\frac{1}{2}(A-3)\,f(z,z',-1) - f(z,z',-\frac{1}{2})\right], \tag{2.52}$$

for the symmetric and mixed-symmetric states. The spatial components reduce to

$$\Pi^{S}(z,r) = F^{S}(z,r) + 2\int_{-1}^{+1} f(z,z',-\frac{1}{2})\,F^{S}(z',r)\,dz' \tag{2.53}$$

$$\Pi^{S'}(z,r) = F^{S'}(z,r) - \int_{-1}^{+1} f(z,z',-\frac{1}{2})\,F^{S'}(z',r)\,dz' \tag{2.54}$$

for three-nucleon systems (Triton) and

$$\Pi^S(z,r) = F^S(z,r) + \int_{-1}^{+1} \left[f(z,z',-1) + 4\, f(z,z',-\frac{1}{2}) \right] F^S(z',r)\, dz' \quad (2.55)$$

$$\Pi^{S'}(z,r) = F^{S'}(z,r) + \int_{-1}^{+1} \left[f(z,z',-1) - 2\, f(z,z',-\frac{1}{2}) \right] F^{S'}(z',r)\, dz' \quad (2.56)$$

for four-nucleon system (α nucleus). Naturally, wavefunction will lead to coupled integrodifferential equations for the symmetric amplitudes $F^S(z',r)$ and mixed-symmetric amplitudes $F^{S'}(z',r)$.

Without loss of generality, we consider only even parity states. Considering nucleon spins and isospin, nuclear potentials with these degrees-of-freedom will involve singlet and triplet components resulting from spin and isospin coupling. The even-parity component of the central spin-dependent nucleon-nucleon interaction has the form

$$V^+(r_{ij},\sigma,\tau) = V^{1+}(r_{ij})\, P_{ij}^{1+} + V^{3+}(r_{ij})\, P_{ij}^{3+} \quad (2.57)$$

where P_{ij}^{1+} and P_{ij}^{3+} are projection operators acting on the singlet-even (1+) and triplet-even (3+) spin states, respectively. The evaluation of matrix elements of this potential with the spin-dependent amplitudes is shown in [38]. The result is a set of two coupled integrodifferential equations [38]

$$\left[\frac{\hbar^2}{m}\nabla_0^2 - N_p\, V_0(r) + E\right] F^S(z,r) = \frac{1}{2}\left[\, V^{1+}(r,z) - V^{3+}(r,z)\,\right] \Pi^{S'}(z,r)$$
$$+ \left[\frac{1}{2}\left[\, V^{1+}(r,z) + V^{3+}(r,z)\,\right] - V_0(r)\right] \Pi^S(z,r) \quad (2.58)$$

$$\left[\frac{\hbar^2}{m}\nabla_0^2 - N_p\, V_0(r) + E\right] F^{S'}(z,r) = \frac{1}{2}\left[\, V^{1+}(r,z) - V^{3+}(r,z)\,\right]\Pi^s(z,r)$$
$$+ \left[\frac{1}{2}\left[\, V^{1+}(r,z) + V^{3+}(r,z)\,\right] - V_0(r)\right] \Pi^{S'}(z,r) \quad (2.59)$$

where

$$V_0(r) = \frac{1}{2\pi}\int_{-1}^{+1} \left[\, V^{1+}(r,z) + V^{3+}(r,z)\,\right] \sqrt{1-z^2}\, dz\,. \quad (2.60)$$

The following matrix elements [38]

$$\langle A \,|\, P_{ij}^{+1} |\,|\, A \rangle = \langle A'_{ij} \,|\, P_{ij}^{+1} |\,|\, A'_{ij} \rangle = \frac{1}{2}\,, \tag{2.61}$$

which hold for P_{ij}^{+3}, were used and

$$\langle A \,|\, P_{ij}^{+1} |\,|\, A'_{ij} \rangle = -\langle A \,|\, P_{ij}^{+3} |\,|\, A'_{ij} \rangle = \frac{1}{2} \tag{2.62}$$

which also hold $\langle A' \,|\, P_{ij}^{+n} |\,|\, A \rangle$ $(n = +1, +3)$. The equations (2.58) and (2.59) are solved directly using the Lagrange-mesh method as explained in the next section.

Chapter 3

The Lagrange-mesh Method

3.1 The variational approach

We briefly outline the numerical approach we adopted to construct numerical solutions to the few-body integrodifferential equations derived in the previous chapter. Consider the Schrödinger equation

$$\hat{H}\,\psi = E\,\psi \tag{3.1}$$

where $\hat{H}$ is the Hamiltonian, E the energy and the wavefunction ψ of a given system. The wavefunction and energy are not known and are to be determined. In the variational approach, the wavefunction is approximated by a linear combination of known basis functions $|i\rangle$ in the form

$$|\psi\rangle = \sum_{i=1}^{\infty} c_i\,|i\rangle \tag{3.2}$$

where c_i are variational parameters. If equation (3.2) is used in equation (3.1), we obtain

$$\hat{H}\sum_{i=1}^{\infty} c_i\,|i\rangle = E\sum_{i=1}^{\infty} c_i|i\rangle\,. \tag{3.3}$$

If we take the inner product with $\langle j|$, we get

$$\sum_{i=1}^{\infty} c_j^* c_i\langle j|\,\hat{H}\,|i\rangle = E\sum_{i=1}^{\infty} c_j^* c_i\langle j|i\rangle\,. \tag{3.4}$$

The variational conditions for making $\langle\hat{H}\rangle$ stationary are [1]

$$\frac{\partial\langle\hat{H}\rangle}{\partial c_j^*} = 0 \qquad \text{and} \qquad \frac{\partial\langle\hat{H}\rangle}{\partial c_i} = 0 \tag{3.5}$$

which lead to a matrix eigenvalue problem

$$\sum_{j=1}^{\infty} c_j \langle j|\hat{H}|i\rangle = E \sum_{j=1}^{\infty} c_i \langle j|i\rangle \,. \tag{3.6}$$

If the basis functions form a complete set of orthogonal functions such that

$$\langle j|i\rangle = \delta_{ij} \,, \tag{3.7}$$

then equations (3.6) take the form

$$\sum_{j=1}^{N} c_j \,\langle j|\,\hat{H}\,|i\rangle = E\, c_i \tag{3.8}$$

where, for numerical implementation, the infinite set of basis is truncated to some number of terms N. The above discussion summarises the theory behind thee variational approximation to eigenvalue problems. In this work we use the Lagrange-mesh bases functions.

The Lagrange-mesh method is a variational method that employs Lagrange functions as bases functions. Such bases functions are defined on some mesh, orthonomalized, infinitely differentiable, and vanish at all mesh points except one [3]. The Lagrange-mesh method use Gauss quadrature as the mesh points. The Lagrange-mesh method has been found to be very accurate but simple even in complicated and realistic problems in atomic [58, 59, 60] and nuclear physics [61, 62, 63]. However, the method does not always work. Its accuracy is affected by the validity of the Gauss quadrature which is affected by singularities or discontinuities of the potentials [3]. This can be remedied in some cases by regularisation of the singularities. But in many cases inaccuracies persist [64].

A Lagrange-mesh function $f_i(x)$ is defined over an interval $x \in [a, b]$ on a mesh x_i ($i = 1, 2, 3, \ldots, N$) associated with a Gauss quadrature of abscissas x_i and weights

λ_i. The Lagrange functions have the properties [3, 47]

$$f_j(x_i) = \lambda_i^{-1/2}\,\delta_{ij} \tag{3.9}$$

$$\int_a^b f_i(x)\,V(x)\,f_j(x)\,dx = V(x_i)\,\delta_{ij} \tag{3.10}$$

$$\int_a^b f_i(x)\,f_j^{(k)}(x)\,dx = \lambda_i^{1/2}\,f_j^{(k)}(x_i) \tag{3.11}$$

where λ_i are integration weights, $V(x)$ a scalar function, δ_{ij} the Kronecker delta, and $f^{(k)} = d^k f/dx^k$ for $k = 1, 2$. These properties of the Lagrange-mesh basis enable the evaluation of matrix elements of quantum mechanics operators in compact form and reduce quantum mechanical equations to a set of algebraic equations [47].

A simple example of the application of the Lagrange-mesh basis functions is presented by a one-dimensional Schrödinger equation

$$\left[-\frac{d^2}{dx^2} + V(x)\right]\,\psi(x) = E\,\psi(x)\,, \qquad x \in [a, b]\,. \tag{3.12}$$

As explained earlier, the wavefunction is approximated by the expansion

$$\psi(x) = \sum_{i=1}^{N} c_j\,f_j(x) \tag{3.13}$$

where c_j are variational parameters and $f_j(x)$ the Lagrange basis functions that are defined on the mesh $a < x_j < b$ ($j = 1, 2, 3, \ldots, N$). The matrix elements operators in equation (3.12) are calculated from

$$\langle\psi(x)\,|\,\psi''(x)\rangle + \langle\psi(x)|\,V(x)\,|\psi(x)\rangle = E\,\langle\psi(x)\,|\,\psi(x)\rangle\,. \tag{3.14}$$

where $\psi'' \equiv d^2\psi/dx^2$. Using properties of the Lagrange functions we obtain a set of algebraic equations

$$\sum_{j=1}^{N}\left[-\lambda^{1/2}\,f_j''(x_i) + V(x_i)\,\delta_{ij}\right]\,c_j = E\,c_i \tag{3.15}$$

where $f_j''(x_i)$ can be computed in compact form. Note that the explicit form of the Lagrange functions is not always required. We apply the same procedure to the solution of the couple integrodifferential equations discussed in the previous chapter.

3.2 The integrodifferential equations

We construct numerical solutions to the few-body integrodifferential equations developed in the previous chapter. The integrodifferential equations to be solved are

$$\begin{aligned}
[\,H_0+E\,]\,F^S(z,r) &= \frac{1}{2}\big[\,V^{1+}(r,z)+V^{3+}(r,z)\,\big]\,\Pi^S(z,r) \\
&+ \frac{1}{2}\big[\,V^{1+}(r,z)-V^{3+}(r,z)\,\big]\,\Pi^{S'}(z,r) \qquad (3.16)\\
[\,H_0+E\,]\;F^{S'}(z,r) &= \frac{1}{2}\big[\,V^{1+}(r,z)+V^{3+}(r,z)\,\big]\Pi^{S'}(z,r) \\
&+ \frac{1}{2}\big[\,V^{1+}(r,z)-V^{3+}(r,z)\,\big]\,\Pi^{S}(z,r) \qquad (3.17)
\end{aligned}$$

where $H_0 = T_r + \frac{4}{r^2}\,T_z$. The equations are solved with the normalization [36]

$$\langle\Psi\,|\,\Psi\rangle = C_A\int_0^\infty dr\,r^{D-1}\int_{-1}^{+1}dz\,w(z)\,\Big[\,F^S(z,r)\,\Pi^S(z,r)+F^{S'}(z,r)\,\Pi^{S'}(z,r)\,\Big] \quad (3.18)$$

where $C_A = 2^{-D/2}\,A(A-1)\,\pi^{(D-3)/2}/\Gamma\left(\frac{D-3}{2}\right)$ is a constant. It is not difficult to include $V_0(r)$ in what follows. To express the equations (3.16) and (3.17) in matrix form, it is convenient to introduce

$$\begin{aligned}
\Pi(z,r) &= \left[\,F(z,r)+\int_{-1}^{+1}f(z,z')\,F(z',r)\,w(z')\,dz'\right] \qquad (3.19)\\
&= \left[\,1+\int_{-1}^{+1}dz'\,w(z')\,f(z,z')\int_{-1}^{+1}dz\,\delta(z-z')\right]F(z,r) \qquad (3.20)\\
&= g(z,z')\,F(z,r) \qquad (3.21)
\end{aligned}$$

where the delta function $\delta(z-z')$ is meant to sift out the values z' in $F(z,r)$. We then cast the equations in the form

$$\begin{bmatrix} H_0-V_{11}(r,z)\,g(z,z') & -V_{12}(r,z)\,g(z,z') \\ -V_{21}(r,z)\,g(z,z') & H_0-V_{22}(r,z)\,g(z,z') \end{bmatrix}\begin{bmatrix} F^S(z,r) \\ F^{S'}(z,r)\end{bmatrix} = -E\begin{bmatrix} F^S(z,r) \\ F^{S'}(z,r)\end{bmatrix} \quad (3.22)$$

where $V_{11} = V_{22} = \frac{1}{2}(\,V^{1+}+V^{3+}\,)$ and $V_{12} = V_{21} = \frac{1}{2}(\,V^{1+}-V^{3+}\,)$. Now the implementation of the Lagrange-mesh bases is easy to explain. Next, we construct the approximate numerical amplitudes $F^S(r,z)$ and $F^{S'}(r,z)$.

There are a number of possible Lagrange functions that can be used to approximate the two-body amplitudes. An extensive discussion of such bases functions can be found in [3]. In this work, we expand the symmetric and mixed-symmetric two-body amplitudes $F^k(r,z)$ $(k = S, S')$ in terms of products of regularised Lagrange-Laguerre $\hat{R}_i(r)$ and Lagrange-Jacobi $\hat{U}_j(z)$ bases functions in the hyperradial and parameterised angular variables, respectively. For N_r and N_z number of bases we have

$$F^k(z,r) = h^{-1/2} \sum_{i=1}^{N_r} \sum_{j=1}^{N_z} C_{ij}^k \, \hat{R}_i(r/h) \, \hat{U}_j(z) \tag{3.23}$$

where h is a scaling factor, which is a free parameter, and C_{ij}^k variational parameters. The effect of the factor h is to reduce the infinite range of the Laguerre functions to the problem domain which is defined by the range of the potential in the hyperradial domain.

The reader is refered [3] for a detailed discussion of Lagrange-Laguerre basis functions.

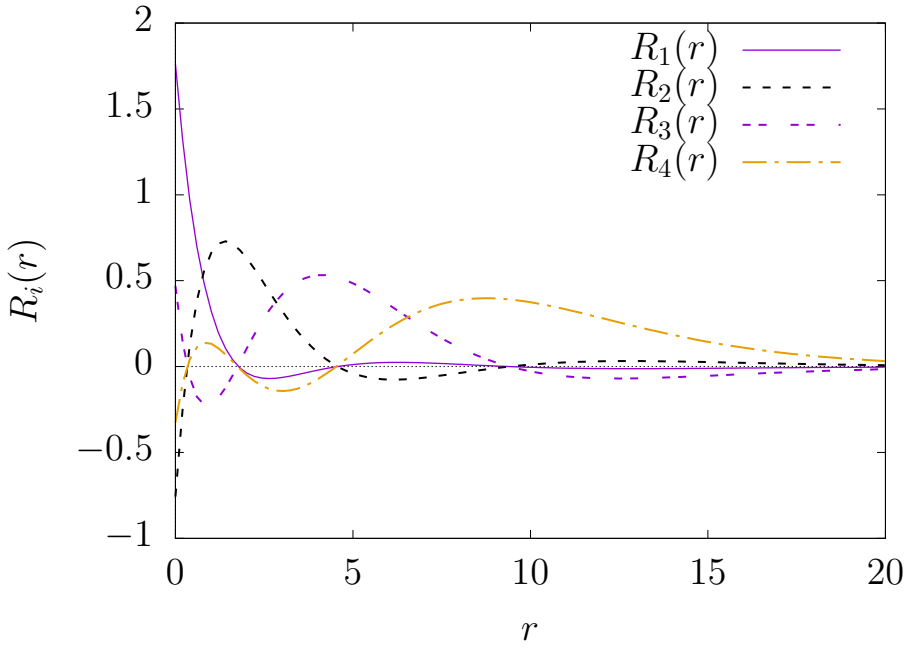

Figure 3.1: A plot of the Lagrange-Laguerre functions $R_N(r)$ for $N = 4$ and $\sigma = 0$.

The Lagrange-Laguerre functions of order N_r have the form [3]

$$R_i(r) = (-1)^i \sqrt{\frac{1}{r_i\, h^\sigma_{N_r}}}\, r^{\sigma/2} e^{-r/2}\, \frac{L^\sigma_{N_r}(r)}{r - r_i} \tag{3.24}$$

where $h^\sigma_{N_r}$ is the normalisation coefficient and the r_i ($i = 1, 2, \ldots, N_r$) the roots of the Laguerre polynomial $L^\sigma_{N_r}(r)$. That is,

$$L^\sigma_{N_r}(r_i) = 0 \tag{3.25}$$

and

$$h^\sigma_{N_r} = \frac{\Gamma(N_r + \sigma + 1)}{\Gamma(N_r + 1)}\,. \tag{3.26}$$

Figure 3.1 displays the Lagrange-Laguerre functions $R_4(r)$ for $N_r = 4$. The choice of the parameter σ is guided by the boundary conditions to be satisfied by $R_i(r)$. Singularities in the r domain require that the Lagrange-Laguerre basis be regularised. The regularization with a factor r, leads to functions of the form

$$\hat{R}_i(r) = \frac{r}{r_i}\, R_i(r) = (-1)^i \sqrt{\frac{r_i}{h^\sigma_{N_r}}}\, r^{\sigma/2+1} e^{-r/2}\, \frac{L^\sigma_{N_r}(r)}{r - r_i}\,, \tag{3.27}$$

that have the same properties as $R_i(r)$ does.

The reader is refered [3, 69] for a detailed discussion of Lagrange-Jacobi basis functions. The Lagrange-Jacobi functions of order N_z are defined by [64]

$$U_j(z) = (-1)^{N_z - j} \left[\frac{(1 - z_j^2)\, w^J(z)}{h^{\alpha,\beta}_{N_z}(2\, N_z + \gamma)}\right]^{1/2} \frac{P^{\alpha,\beta}_{N_z}(z)}{z - z_j} \tag{3.28}$$

where $\gamma = \alpha + \beta + 1$, $w^J(z) = (1 - z)^\alpha (1 + z)^\beta$, $h^{\alpha,\beta}_{N_z}$ the normalisation coefficient and z_j ($j = 1, 2, \ldots, N_z$) the roots of the Jacobi polynomials $P^{\alpha,\beta}_{N_z}(z)$. That is,

$$P^{\alpha,\beta}_{N_z}(z_j) = 0 \tag{3.29}$$

and

$$h^{\alpha,\beta}_{N_z} = \frac{2^\gamma}{2N_z + \gamma} \frac{\Gamma(N_z + \alpha + 1)\Gamma(N_z + \beta + 1)}{\Gamma(N_z + 1)\,\Gamma(N_z + \gamma)}\,. \tag{3.30}$$

Figure 3.2 shows the Lagrange-Jacobi functions $U_4(z)$ for $N_r = 4$. Regularisation with a factor $w_r(z) = (1-z)^a(1+z)^b$ leads for functions of the form

$$\hat{U}_j(z) = \frac{w_r(z)}{w_r(z_j)}\, U_j(z) = (-1)^{N_z - j} \left[\frac{(1-z_j^2)\, w^J(z)\, w_r(z)}{h^{\alpha,\beta}_{N_z}(2\,N_z + \gamma)\, w_r(z_j)} \right]^{1/2} \frac{P^{\alpha,\beta}_{N_z}(z)}{z - z_j} \tag{3.31}$$

where (a, b) are the regularisation parameters. The choice of the parameters (a, b) motivated by the singularities on the boundaries of the z domain. The functions $\hat{U}_j(z)$ have the same properties as $U_j(z)$ does.

We are now able to evaluate matrix elements of the equations (3.16) and (3.17). The Gauss approximate Lagrange-mesh matrix elements for the radial kinetic energy oper-

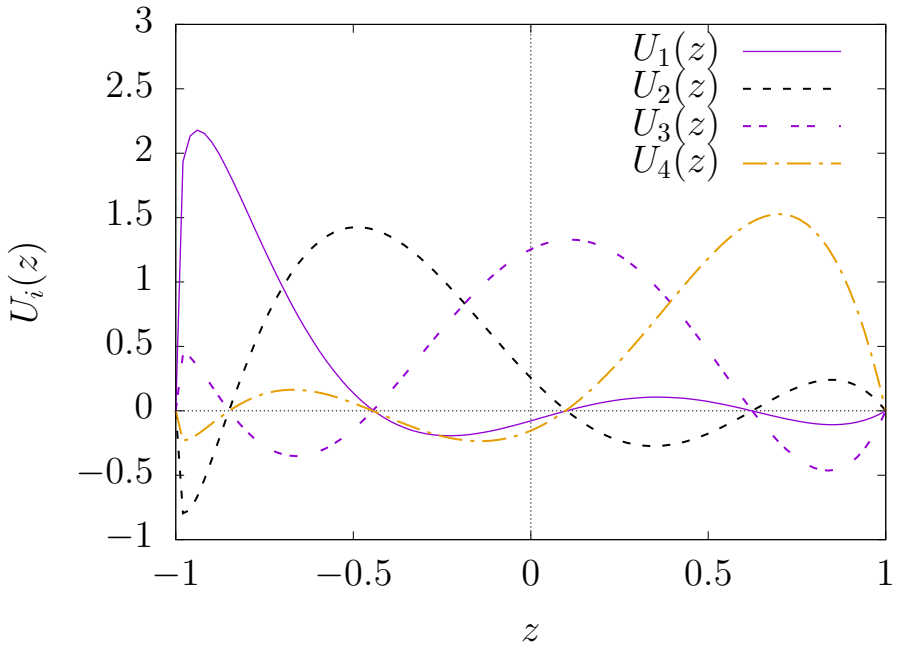

Figure 3.2: A plot of the Lagrange-Jacobi functions $U_N(z)$ for $N = 4$ and $(\alpha, \beta) = (2, \frac{1}{2})$.

ator are given by [2]

$$T^r_{ik} = -\left\langle \hat{R}_k(r) \,\middle|\, \frac{d^2}{dr^2} \,\middle|\, \hat{R}_i(r) \right\rangle \tag{3.32}$$

$$= \begin{cases} (-1)^{i-k} \dfrac{r_i + r_k}{\sqrt{r_i r_k}(r_i - r_k)^2} & ;\ i \neq k \\ \dfrac{4-\sigma^2}{12 r_i^2} + \dfrac{2N_r + \sigma + 1}{6 r_i} - \dfrac{1}{12} & ;\ i = k \end{cases} \tag{3.33}$$

which are compact functions of the mesh points r_i. The Gauss approximate Lagrange-mesh matrix elements for the parametric angular kinetic energy operator are given by [64]

$$\mathcal{T}^z_{ij} = \left\langle \hat{U}_l(z) \,\middle|\, \frac{1}{w_0(z)} \frac{\mathrm{d}}{\mathrm{d}z} (1-z^2)\, w_0(z) \frac{\mathrm{d}}{\mathrm{d}z} \,\middle|\, \hat{U}_j(z) \right\rangle \tag{3.34}$$

$$= \begin{cases} (-1)^{i-j} \dfrac{w_s(z_i)}{w_s(z_j)} \left[\dfrac{\nu_0 - \nu_1 z_i}{z_i - z_j} - \dfrac{2(1-z_i^2)}{(z_i - z_j)^2} \right] & ; \quad i \neq j \\ \dfrac{1 - (2N_z + \gamma)^2}{12} + \dfrac{\omega_0 + \omega_1 z_i + \omega_2 z_i^2}{12(1-z_i^2)} & ; \quad i = j \end{cases} \tag{3.35}$$

for $w_0(z) = (1-z)^{\alpha_0}(1+z)^{\beta_0}$, where

$$w_s(z) = (1-z)^{(a-1)/2}(1+z)^{(b-1)/2}\,, \tag{3.36a}$$

$$\nu_0 = \beta_0 - \alpha_0 + b - a\,, \tag{3.36b}$$

$$\nu_1 = \beta_0 + \alpha_0 + b + a \tag{3.36c}$$

and

$$\omega_0 = 2(\alpha^2 + \beta^2) + 3(\nu_0 + \beta_0 - \alpha_0)(b-a) - 6(a+b) + 8\,, \tag{3.37a}$$

$$\omega_1 = 2(\alpha^2 - \beta^2) - 6\nu_0(a+b-2) + 6(\beta_0 + \alpha_0)(a-b)\,, \tag{3.37b}$$

$$\omega_2 = 3(\nu_1 + \beta_0 + \alpha_0)(a+b-2) \tag{3.37c}$$

are defined. As can be seen, the matrix elements (3.35) are compact functions of the mesh points z_i.

The matrix form of (3.16) and (3.17) involves the matrix elements

$$H^0_{ij,kl} = \frac{\hbar^2}{m h^2} \left[T^r_{ik}\, \delta_{jl} - \frac{1}{r_i^2} \left(4\, T^z_{jl} - \frac{1}{4}\, \delta_{jl} \right) \delta_{ik} \right] \tag{3.38}$$

$$V^{nm}_{ij,kl} = \left[\delta_{jl} + \sqrt{\lambda_j\, \lambda_l\, w(z_j)}\, f(z_l, z_j) \right] V_{nm}(h\, r_i, z_j)\, \delta_{ik} \tag{3.39}$$

where $n, m = \{\, 1, 2 \,\}$ and $\lambda_j = w_j^J / w(z_j)$ with w_j^J as Gauss-Jacobi quadrature weights. The matrix eigenvalue problem to be solved is

$$\sum_{kl} \begin{bmatrix} H^0_{ij,kl} - V^{11}_{ij,kl} & -V^{12}_{ij,kl} \\ -V^{21}_{ij,kl} & H^0_{ij,kl} - V^{22}_{ij,kl} \end{bmatrix} \begin{bmatrix} C^S_{kl} \\ C^{S'}_{kl} \end{bmatrix} = -E \begin{bmatrix} C^S_{ij} \\ C^{S'}_{ij} \end{bmatrix} . \tag{3.40}$$

The hypercentral potential is included by simply adding $N_p\, V_0(h\, r_i)\, \delta_{jl}$ to (3.38) and replacing $V_{nm}(h\, r_i, z_j)$ with $V_{nm}(h\, r_i, z_j) + V_0(h\, r_i)\, \delta_{jl}$ in (3.39). A standard matrix diagonalization routine is used to determine E and the variational parameters C^S and $C^{S'}$. The normalisation (3.18) dictates that [64]

$$\sum_{\kappa ij} \left(C^\kappa_{ij}\right)^* \left[C^\kappa_{ij} + \sum_l f_\kappa(z_j, z_l)\, C^\kappa_{il} \right] = 1 \tag{3.41}$$

where $\kappa = S, S'$.

Chapter 4

Results and Discussions

4.1 Nuclear interaction potentials

Theoretical studies of nuclear systems require potential models as input to describe interactions in the system. A number of two-body and three-body interaction potential models have been constructed from fitting experimental nucleon-nucleon scattering data. Such potential models are phenomenological and are often called realistic nuclear potential models. Traditional potential models are still useful in testing the effectiveness of new numerical approaches in constructing solutions to quantum mechanical equations. There are results generated with such potentials in the literature that enable comparisons.

In this dissertation we consider the soft-core spin-dependent S3 [65] and S4 [66] potentials. The singlet and triplet components of these potentials are constructed from a superposition of three Gaussian form factors [65]

$$\begin{aligned} V_t(r) &= 1000\, e^{-3.0\, r^2} - 326.7\, e^{-1.05\, r^2} - 43\, e^{-0.60\, r^2} \\ V_s(r) &= 1000\, e^{-3.0\, r^2} - 166\, e^{-0.8\, r^2} - 23\, e^{-0.4\, r^2} \end{aligned} \tag{4.1}$$

for the S3 potential, and [66]

$$\begin{aligned} V_t(r) &= 600\, e^{-5.5\, r^2} - 70\, e^{-0.5\, r^2} - 27.6\, e^{-0.38\, r^2} \\ V_s(r) &= 880\, e^{-5.4\, r^2} - 70\, e^{-0.64\, r^2} - 21\, e^{-0.48\, r^2} \end{aligned} \tag{4.2}$$

for the S4 potential. Figure 4.1 and 4.2 display the form of the S3 and S4 components,

respectively.

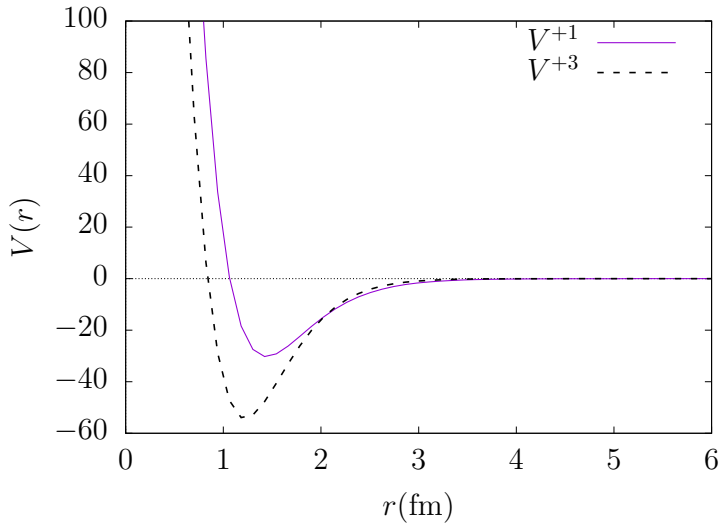

Figure 4.1: The graphs of the singlet and triplet components of the S3 potential

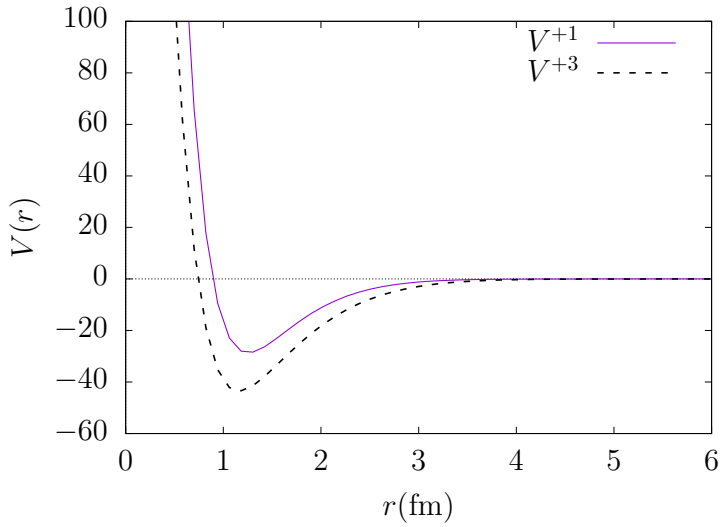

Figure 4.2: The graphs of the singlet and triplet components of the S4 potential

We also consider a hard-core spin-dependent Malfiet-Tjon (MT I-III) potential [67, 68]. The singlet and triplet components of this potential are constructed from a superposi-

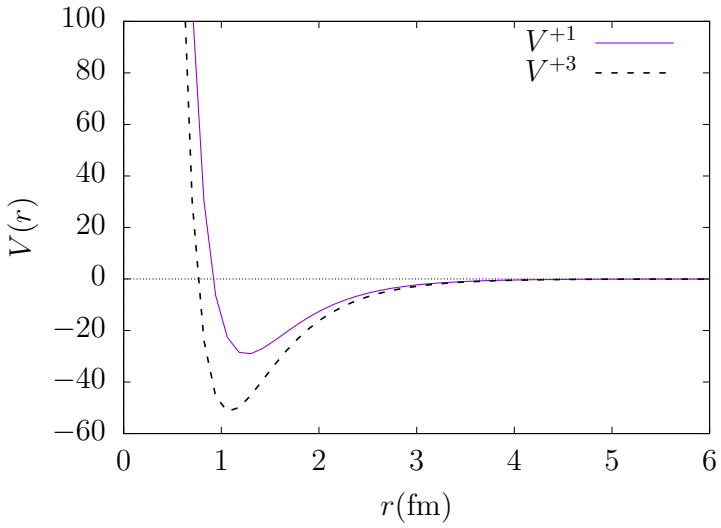

Figure 4.3: A plot of the singlet and triplet components of the MT I-III potential

tion of two Yukawa form factors [67]

$$\begin{aligned} V_t(r) &= \frac{1}{r}\left(1438.72\, e^{-3.11\, r} - 626.885\, e^{-1.55\, r}\right) \\ V_s(r) &= \frac{1}{r}\left(1438.72\, e^{-3.11\, r} - 513.968\, e^{-1.55\, r}\right) \end{aligned} \tag{4.3}$$

and have a singularity at the origin. The two components are displayed in Figure 4.3. We compare the singlet and triplet form factors of the three potentials in Figure 4.4 and 4.5, respectively.

Parameters required as input in the calculations are the scaling factor h, the regularisation parameters (a, b), the range of the hyperradial domain r_{max}, and the bases size (N_r, N_z). The mass of the nucleon was chosen such that $\hbar^2/m = 41.47\,\text{MeV}$ in all the cases. The problem domain is defined by r and z. We set $z \in [\,-1, +1\,]$ and $r \in [\,0, r_{max}\,]$ were r_{max} is determined by the potential range. We chose $r_{max} = 20\,\text{fm}$. The parameter of the Lagrange-Laguerre functions was set to $\sigma = 0$ since the Laguerre functions were regularised. The Lagrange-Jacobi parameters were set to $(\alpha, \beta) = (\frac{1}{2}, \frac{1}{2})$ for the three-body system and $(\alpha, \beta) = (2, \frac{1}{2})$ for the four-body system with $(a, b) = (\frac{1}{2}, \frac{1}{2})$ for both systems. The scaling parameter was set to $h = r_{max}/x_N$ where x_N is the largest root of the Laguerre polynomial. The bases size (N_r, N_z) was varied.

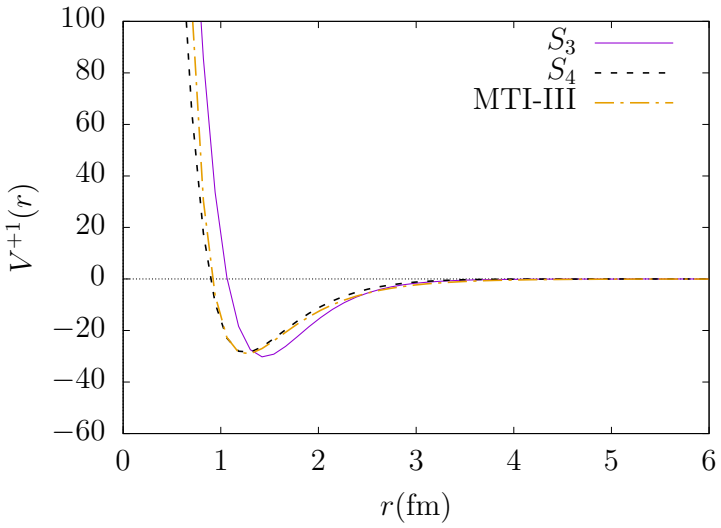

Figure 4.4: Comparison of the singlet components of the three potentials

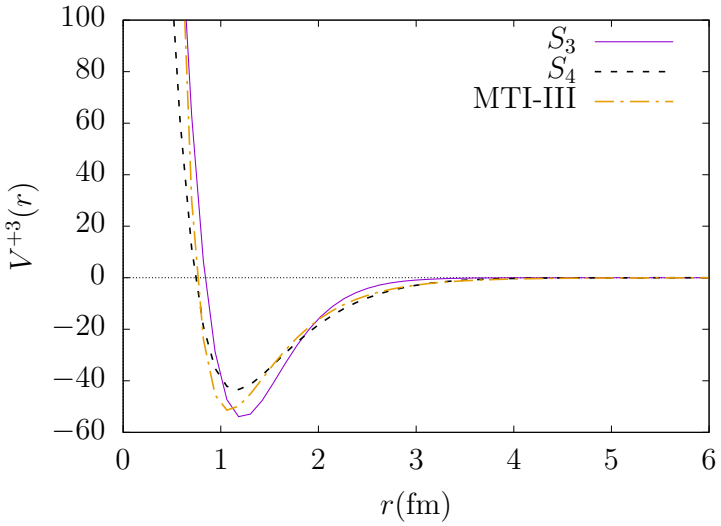

Figure 4.5: Comparison of the triplet components of the three potentials

4.2 The Triton nucleus: 3-body system

We first calculated the ground-state energy E_0 (MeV) of the Triton (^{3}H) nucleus interacting through the spin-averaged potentials with different bases sizes $N = N_r = N_z$. Only a single two-variable integrodifferential equation was solved in these cases and the results are referred to as single-channel results. Converged two-channel results are discussed at the end of the section.

4.2.1 The S3 potential

In Table 4.1 we show the values of the calculated ground-state energy $-E_0$ (MeV) as a function of the bases size N for the rSIDE and rIDEA cases. The total bases size is, therefore, N^2. As can be deduced from the table, the magnitude of the ground-state energy decrease from 9.13862 MeV to 6.40914 MeV when N increase from 20 to 40, for rSIDE. The variation of the rIDEA ground-state energy is similar to that of rSIDE. The energy decreases from 9.28619 MeV to 6.6756 MeV when N increases from 20 to 40. The rate of convergence of the energy with increase in the bases is illustrated in Figure 4.6. As seen from the figure convergence is rapid for both rSIDE and rIDEA energies. This rapid convergence shows the efficiency of the Lagrange-mesh method in the numerical solution of the coupled two-variable integrodifferential equations.

Table 4.1: Variation of the ground-state energy $-E_0$ (MeV) of ^{3}H interacting through the S3 potential as $N = N_r = N_z$ is varied, for rSIDE and rIDEA.

N	rSIDE	rIDEA
10	8.208036	8.591300
15	7.951308	8.219450
20	9.138618	9.286189
25	8.505835	8.606028
30	6.409189	6.675655
35	6.409165	6.675655
40	6.409141	6.675600

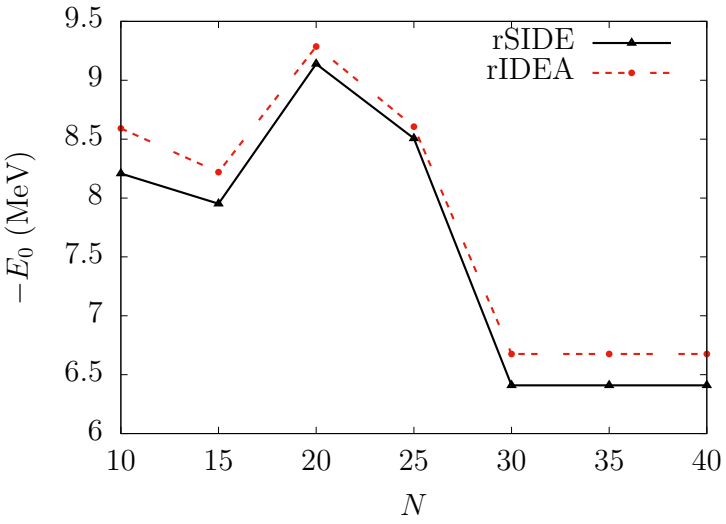

Figure 4.6: A plot of the variation of the ground-state energy with the change in the bases size N from Table 4.1: ^{3}H nucleus interacting with S3 potential.

4.2.2 The S4 potential

In Table 4.2 we show the values of the calculated ground-state energy $-E_0\,(\mathrm{MeV})$ as a function of the bases size N for the three-nucleon system interacting through the spin-dependent S4 nucleon-nucleon potential. The values given are for the rSIDE and rIDEA cases. From the table, the rSIDE results show that the magnitude of the ground-state energy decreases from 7.54363 MeV to 6.9291 MeV as N increase from 10 to 40. The calculated rIDEA ground-state energy decreases from 7.73381 MeV to 7.083513 MeV when N increases from 10 to 40. The rate of convergence of the energy with increase in the bases is illustrated in Figure 4.7m which show that the rate of convergence is rapid for both rSIDE and rIDEA energies. The rapid convergence is an indication of the efficiency of the Lagrange-mesh method in constructing numerical solutions to the coupled two-variable few-body integrodifferential equations.

Table 4.2: Variation of the ground-state energy $-E_0$ (MeV) of ^{3}H interacting through the S4 potential as N is varied, for rSIDE and rIDEA.

N	rSIDE	rIDEA
10	7.543630	7.733812
15	6.995604	7.153727
20	6.935309	7.089894
25	6.929172	7.083563
30	6.928897	7.083311
35	6.929022	7.083447
40	6.929085	7.083513

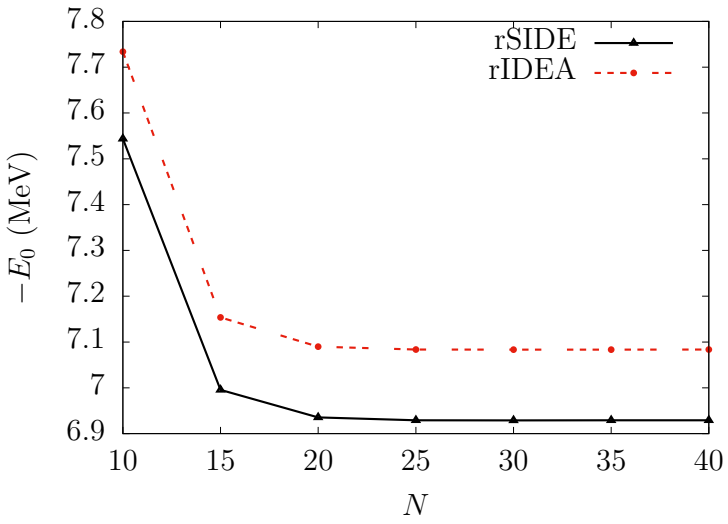

Figure 4.7: A plot of the variation of the ground-state energy with the change in the bases size from Table 4.2: ^{3}H nucleus interacting with S4 potential.

4.2.3 The MT I-III potential

We calculated the ground-state energy of the Triton nucleus interacting through the spin-dependent MT I-III nucleon-nucleon potential with different bases sizes $N = N_r =$

N_z. In Table 4.3, we show the calculated ground-state energy $-E_0$ (MeV) as a function of the bases size for the rSIDE and rIDEA cases. We can deduce from the table that the magnitude of the ground-state energy decrease from 8.97235 MeV to 7.55809 MeV when N increase from 20 to 40, for rSIDE. The variation of the rIDEA ground-state energy is similar to that of rSIDE. The energy decreases from 9.15666 MeV to 7.70362 MeV when N increases from 20 to 40. The rate of convergence of the energy with increase in the bases is illustrated in Figure 4.8. As seen from the figure, the rate of convergence of the calculated energies is not as rapid, for both rSIDE and rIDEA, as in the other two potentials. Convergence may be slow because of the occurrence of the hard-core and singularity in the MT I-III potential.

Table 4.3: Variation of the ground-state energy $-E_0$ (MeV) of ^{3}H interacting through the MT I-III potential as $N = N_r = N_z$ is varied, for rSIDE and rIDEA.

N	rSIDE	rIDEA
10	8.972348	9.156665
15	7.914920	8.068102
20	7.666235	7.812361
25	7.598235	7.743558
30	7.574333	7.719689
35	7.563705	7.709157
40	7.558088	7.703616

4.2.4 Summary of results for Triton

We summarise the rSIDE and rIDEA converged results for the three potentials. In Table 4.4, we present results for the spin-averaged potentials with those reported in

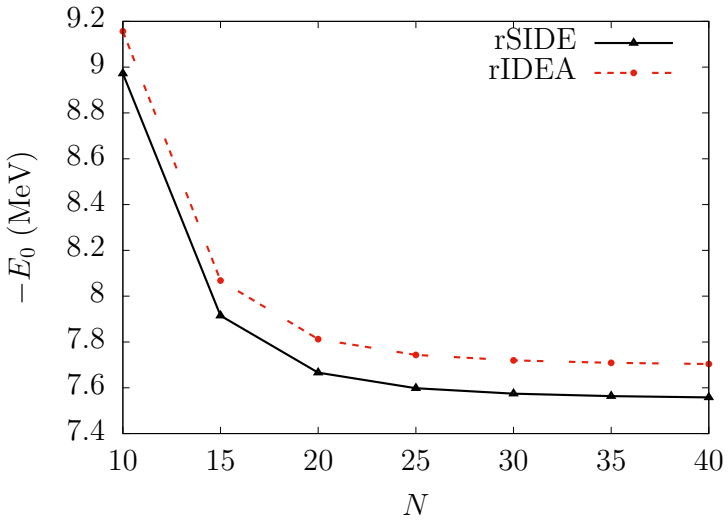

Figure 4.8: A plot of the variation of the ground-state energy with the change in the bases size from Table 4.3: ^{3}H nucleus interacting with MT I-III potential.

the literature obtained with similar methods. Our rSIDE energies are 6.409 MeV, 6.929 MeV and 7.558 MeV for the S3, S4 and MT I-III potentials, respectively. We obtained rIDEA energies of 8.758 MeV, 7.913 MeV and 8.869 MeV for the S3, S4 and MT I-III potentials, respectively. The rIDEA energies are consistently lower that the rSIDE results for all three potentials. This is expected since the difference emanates from the effects of higher partial waves accounted for in rIDEA. A similar investigation

Table 4.4: Single-channel ground-state energy $-E_0$ (MeV) of Triton.

	S3	S4	MT I-III
rSIDE	6.409 141	6.929 085	7.558 088
SIDE [37]	6.41	6.93	
Faddeev [39]	6.409 128		8.535 784
rIDEA	6.675 66	7.083 31	7.719 69
IDEA [37]	6.67	7.08	

was carried out in [37] where the integrodifferential equations are solved exactly using splines. Our single-channel rSIDE and rIDEA results reproduce those of SIDE and IDEA [37], respectively, for S3 and S4. Our S3 results are also in perfect agreement with the Faddeev results of [39]. However, MT I-III rSIDE results, which showed slow convergence, are lower than the Faddeev results by about 1 MeV.

In Table 4.5 we display the two-channel results for the three spin-dependent potentials. We obtained rSIDE energies of 8.201 MeV, 7.604 MeV and 8.542 MeV for the S3, S4 and MT I-III potentials, respectively. Our rIDEA energies are 8.758 MeV, 7.913 MeV and 8.869 MeV for the S3, S4 and MT I-III potentials, respectively. Our S3 and MT I-III results are in agreement with SIDE and IDEA results [37]. The small discrepancies can be attributed to numerical error related to convergence challenges of the Lagrange-mesh method. Similar S4 results are difficult to find in the literature for comparison.

Table 4.5: Two-channel ground-state energy $-E_0$ (MeV) of Triton.

	S3	S4	MT I-III
rSIDE	8.201 31	7.604 451	8.541 707
SIDE [38]	8.20		8.54
rIDEA	8.758 211	7.913 196	8.869 356
IDEA [37]	8.75		8.86

4.3 The α nucleus: 4-body system

We first calculated the ground-state energy E_0 (MeV) of the α (^{4}He) nucleus interacting through the spin-averaged potentials with different bases sizes $N = N_r = N_z$. The results are referred to as single-channel results. Converged two-channel results are discussed at the end of the section.

4.3.1 The S3 potential

In Table 4.6 we show the values of the calculated ground-state energy $-E_0\,(\mathrm{MeV})$ as a function of the bases size N for the four-nucleon system interacting through the spin-dependent S3 nucleon-nucleon potential. We report the values for the rSIDE and rIDEA cases. From the table, the rSIDE results show that the magnitude of the ground-state energy increases from 23.13453 MeV to 23.8075 MeV as N increase from 10 to 40. The rIDEA ground-state energy increases from 23.22299 MeV to 24.026132 MeV when N increases from 10 to 40. The rate of convergence of the energy with increase in the bases is shown in Figure 4.9, which shows that the rate of convergence is rapid for both rSIDE and rIDEA energies with little variation. The rapid convergence is also an indication of the efficiency of the Lagrange-mesh method in solving these coupled two-variable few-body integrodifferential equations.

Table 4.6: Variation of the ground-state energy $-E_0\,(\mathrm{MeV})$ of ^{4}He interacting through the S3 potential as N is varied, for rSIDE and rIDEA.

N	rSIDE	rIDEA
10	23.134525	23.222990
15	23.795660	24.010093
20	23.809726	24.028316
25	23.807889	24.026483
30	23.807573	24.026167
35	23.807533	24.026133
40	23.807530	24.026132

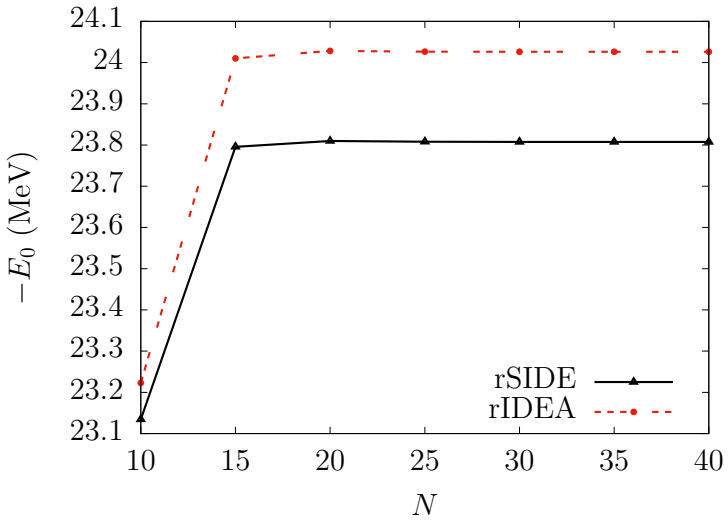

Figure 4.9: A plot of the variation of the ground-state energy with the change in the bases size from Table 4.6: ^{4}He nucleus interacting with S3 potential.

4.3.2 The S4 potential

We calculated the ground-state energy of the α nucleus interacting through the spin-dependent S4 nucleon-nucleon potential with different bases sizes $N = N_r = N_z$. In Table 4.7, we display values of the calculated ground-state energy $-E_0\,(\text{MeV})$ as a function of the bases size N for the rSIDE and rIDEA. It can be seen in the table that the magnitude of the ground-state energy decrease slightly from 26.03799 MeV to 26.0405 MeV when N increase from 10 to 40, for rSIDE. The variation of the rIDEA ground-state energy is similar to that of rSIDE. The energy increases from 27.15161 MeV to 27.27072 MeV when N increases from 10 to 40. The rate of convergence of the energy with increase in the bases is shown in Figure 4.10. As seen from the figure, convergence is quite rapid for both rSIDE and rIDEA energies with very little variation. Again, this rapid convergence shows the efficiency of the Lagrange-mesh method in solving the coupled two-variable integrodifferential equations numerically.

Table 4.7: Variation of the ground-state energy $-E_0$ (MeV) of ^{4}He interacting through the S4 potential as N is varied, for rSIDE and rIDEA.

N	rSIDE	rIDEA
10	26.037990	27.151609
15	26.013397	27.239669
20	26.036957	27.267211
25	26.040340	27.270550
30	26.040559	27.270741
35	26.040542	27.270726
40	26.040532	27.270720

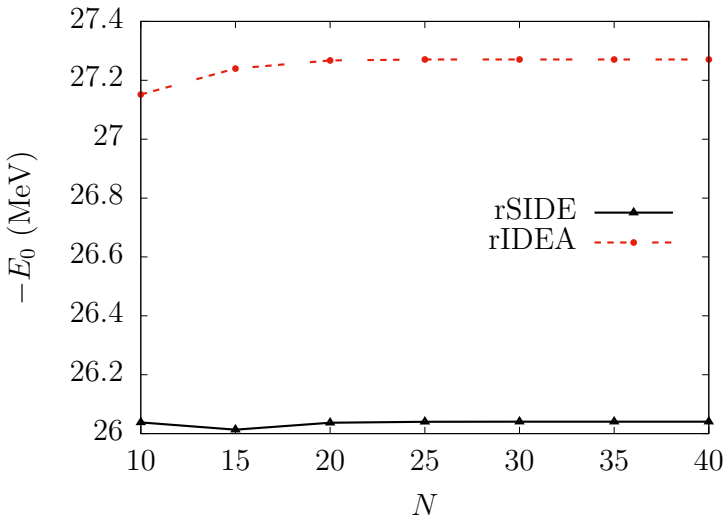

Figure 4.10: A plot of the variation of the ground-state energy with the change in the bases size from Table 4.7: ^{4}He nucleus interacting with S4 potential.

4.3.3 The MT I-III potential

We calculated the ground-state energy of the α nucleus interacting through the spin-dependent MT I-III nucleon-nucleon potential with different bases sizes N. In Table

4.8, we display the calculated ground-state energy $-E_0$ (MeV) as a function of the bases size for the rSIDE and rIDEA cases. We deduce from the table that the magnitude of the ground-state energy decreases from 30.467912 MeV to 26.965642 MeV when N increase from 10 to 40, for rSIDE. The variation of the rIDEA ground-state energy is similar to that of rSIDE. In this rIDEA case, the energy decreases from 31.4241 MeV to 27.7517 MeV when N increases from 10 to 40. The rate of convergence of the energy with increase in the bases is plotted in Figure 4.11. As can be seen from the figure, the rate of convergence of the calculated energies is again not as rapid, for both rSIDE and rIDEA, as in the other two soft-core potentials. The slow convergence may be attributed to the occurrence of the hard-core and singularity in the MT I-III potential.

Table 4.8: Variation of the ground-state energy $-E_0$ (MeV) of ^{4}He interacting through the MT I-III potential as N is varied, for rSIDE and rIDEA.

N	rSIDE	rIDEA
10	30.467912	31.424142
15	27.771219	28.635081
20	27.241412	28.058230
25	27.084250	27.884112
30	27.018481	27.810780
35	26.984949	27.773304
40	26.965642	27.751702

4.3.4 Summary of results for the alpha nucleus

In this section, we summarise the rSIDE and rIDEA converged results for the three potentials in Table 4.9 for the 4-body systems. The converged results are also com-

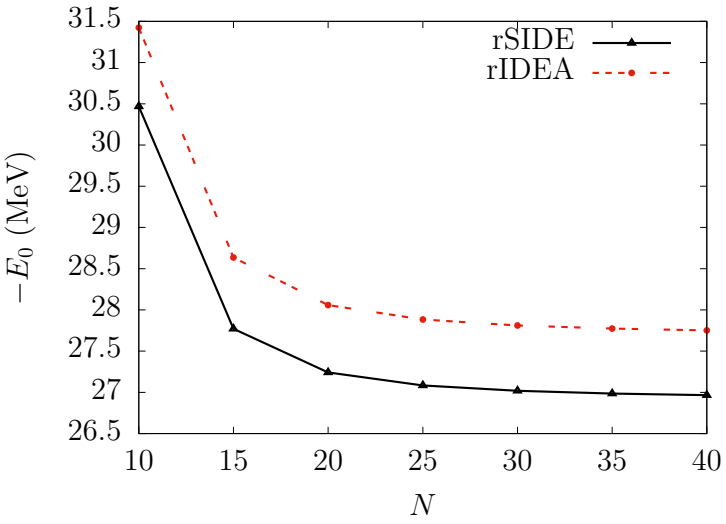

Figure 4.11: A plot of the variation of the ground-state energy with the change in the bases size from Table 4.8: ^{4}He nucleus interacting with MT I-III potential.

pared with those reported in the literature obtained with other methods. We obtained rSIDE energies of 23.808 MeV, 26.041 MeV and 26.966 MeV for the S3, S4 and MT I-III potentials, respectively. The S3 and S4 results are both ∼1.6 MeV lower than the corresponding SIDE results [37]. Our S3 rSIDE results are also 3.4 MeV lower than the Faddeev results [39]. Our rIDEA energies are 24.026 MeV, 27.271 MeV and 27.811 MeV for the S3, S4 and MT I-III potentials, respectively. In this case, our S3 and S4

Table 4.9: Single-channel ground-state energy $-E_0$ (MeV) of α.

	S3	S4	MT I-III
rSIDE	23.807 530	26.040 532	26.965 642
SIDE [37]	25.38	27.74	
Faddeev [39]	25.674 5		30.311 7
rIDEA	24.026 48	27.270 74	27.810 78
IDEA [37]	27.09	28.80	

results are lower than the corresponding SIDE results [37] by ∼3 MeV and ∼1.5 MeV, respectively. Our S3 rSIDE results are also 3.4 MeV lower than the Faddeev results [39]. Literature two-channel results for the MT I-III potential are difficult to find for comparison.

In Table 4.10 we display the two-channel results for the three spin-dependent potentials. We obtained the rSIDE ground-state energies of 26.419 MeV, 26.744 MeV, and 28.255 MeV for the S3, S4 and MT I-III potentials, respectively. The S3 and MT I-III results are both ∼1.5 MeV lower than the corresponding SIDE results [37]. Our S3 rSIDE results are also 2.37 MeV lower than the Faddeev results [39]. The significant and similar discrepancy between our results and those of [37] indicates a possible fault in our implementation of the projection kernel. Such a discrepancy is likely to persist in the case of the S4 potential. We obtained the rSIDE energy of 26.744 MeV and the rIDEA energy of 27.863 MeV for the S4 potential. Again, similar S4 results are difficult to locate in the literature for comparison. The rIDEA S3 and MT I-III results fail to converge. This convergence challenge is hard to explain.

Table 4.10: Two-channel ground-state energy $-E_0$ (MeV) of α.

	S3	S4	MT I-III
rSIDE	26.418 533	26.744 281	28.255 180
SIDE [37]	27.93		29.74
Faddeev [39]	28.784 3		
rIDEA		27.863 194	
IDEA [37]	30.37		31.02

Chapter 5

Concluding Remarks

We studied the ground-state properties of the the Triton and alpha particle systems using the regularised integrodifferential equations approach. The equations depend on only two variables and take into account two-body correlations only. Effects of higher partial waves of the two-body potential are included through an approximation. We used spin-dependent two-body potentials to describe interactions in the system. In such cases, the integrodifferential equations approach leads to couple equations involving symmetric and mixed-symmetric Faddeev-type amplitudes. We used spin-dependent Gaussian-type S3 and S4 nucleon-nucleon potentials as well as the Yukawa-type MT I-III nucleon-nucleon potential.

We solved the system of the coupled integrodifferential equations using Lagrange-mesh method. We used the regularised Lagrange-Laguerre and Lagrange-Jacobi functions as basis functions to solve the system of coupled integrodifferential equations. The solution method led to a matrix eigenvalue problem which was solved using a Fortran program. Unlike most numerical methods, the Lagrange-mesh method result in an eigenvalue problem that does not require a large amount of computer space. We calculated the ground-state energies of the Triton and α particles which are three-body and four-body systems, respectively. The eigenvalue problem was solved using a laptop. We tested the variation of the single-channel energies at different bases sizes where only one equation was solved. We calculated two-channel energies where two coupled equations were solved.

For both Triton and α nuclei, the single-channel rSIDE and rIDEA results showed rapid convergence in the case of the soft-core S3 and S4 Gaussian-type potentials while convergence was comparatively slower for the MT I-III potential. Our results for the Triton are in perfect agreement with the SIDE and IDEA results reported in the literature for the three potentials. This shows the efficiency of the Lagrange-mesh method in solving the few-body integrodifferential equations. Results for the α system show a consistent discrepancy compared to the results reported in the literature. This suggests a possible incorrect implementation of the four-body projection kernel, which requires further investigation.

Our two-channel rSIDE and rIDEA results for the Triton nucleus are also in agreement with those reported in the literature for the three potentials. However, there were challenges with the results for the α nucleus. The rSIDE results are considerably lower that those reported in the literature while the rIDEA results failed to converge for the S3 and MT I-III potentials. This also requires further investigation. No literature results could be found for comparison for the S4 potential. The accuracy our results and the rapid convergence of the solution for the Triton and α nuclei show that the Lagrange-mesh method is a promising method for the investigation of few body systems.

Bibliography

[1] E. Merzbacher: Quantum Mechanics (3rd ed.): Wiley-New York (1998).

[2] G. J. Rampho: J. Phys.: Conf. Ser. **905** 012037 (2017)

[3] D. Baye: Phys. Rep. **565** 1 (2015).

[4] S. Flügge: Practical Quantum Mechanics: Springer-Berlin (1999).

[5] E. Whittaker, S. McCrae: INTEGRATION BY SERIES. In "A Treatise on the Analytical Dynamics of Particles and Rigid Bodies" (Cambridge Mathematical Library, pp. 423-450). Cambridge: Cambridge University Press (1988).

[6] D. J. Griffits: Introduction to Quantum Mechanics: Prentice Hall-New Jersey (1995)

[7] A. Bachkhaznadji, M. Lassaut: Few-body Systems **56**, 1 (2015).

[8] J. Golak, R. Skibińsiki, H. Witala, W. Glöckle, A. Nogga, H. Kammada: Phys. Rep. **415** 89 (2005)

[9] H. P. Noyes, H. Fiedeldey: In "Three-Particle Scattering in Quantum Mechanics" (J. Gillespie, P. M. Rolph, eds.) Benjamin-New York (1968); H. P. Noyes, In "Three-Body Problem in Nuclear and Particle Physics" (J. S. C. McKee, P. M. Rolph, eds.) North-Holland-Amsterdam (1970).

[10] S. P. Merkuriev, S. L. Yakovlev, C. Gignoux: Nucl. Phys. A **431**, 125 (1984).

[11] M. Fabre de La Ripelle, J. Navarro: Ann. Phys. **123**, 185 (1979).

[12] J. L. Ballot, M. Fabre de la Ripelle: Ann. Phys. **127**, 62 (1980).

[13] M. Fabre de la Ripelle, H. Fiedeldey, S. A. Sofianos: Phys. Rev. C **38**, 449 (1988).

[14] M. Fabre de la Ripelle, H. Fiedeldey, S. A. Sofianos: Few-body Syst. **6**, 157 (1989).

[15] M. L. Lekala, G. J. Rampho, S. A. Sofianos, R. M. Adam: Few-Body Syst. **50**, 427 (2010).

[16] G. J. Rampho, S. A. Sofianos, R. M. Adam: Phys. Part. Nucl. **40**, 757 (2009).

[17] S. A. Sofianos, R. M. Adam, V. B. Belyaev: M. Phys. Lett. A **24**, (2009).

[18] R. M. Adam, S. A. Sofianos: Phys. Rev. A **82**, 053635 (2010).

[19] L. D. Faddeev: Sov. Phys JETP. **12**, 1014 (1961).

[20] J. Carbonell, C. Gignoux, S. P. Merkuriev: Few-Body Syst. **15** 15 (1993).

[21] A. K. Motovilov: Few-Body Syst. **43**, 121 (2008).

[22] H. Fiedeldey: Nucl. Phys. A **463**, 335c (1987).

[23] T.E. Mdlalose, H. Fiedeldey, and W. Sandhas: Phys. Rev. C **33**, 784 (1986).

[24] F. Zernike, H. C. Brinkman: Proc. K. Ned. Akad. Wett. **38**, 161 (1935).

[25] L. M. Delves: Nucl. Phys. **9**, 391 (1959); **20**, 275 (1960).

[26] Yu. A. Simonov: Sov. J. Nucl. Phys. **3**, 461 (1966).

[27] F. T. Smith: Phys. Rev. **120**, 1058 (1960); J. Math. Phys. **3**, 735 (1962).

[28] M. Viviani, A. Kievsky, S. Rosati: II Nov. Cim. A **105**, 1473 (1992).

[29] R. Krivec: Few-Body Systems **25**, 199 (1998).

[30] M. I. Haftel, V. B. Mandelzwig: Phys. Lett. A **120**, 232 (1987).

[31] M. I. Haftel, V. B. Mandelzwig: Ann. Phys. **189**, 29 (1985); **195**, 420 (1989).

[32] Y. Wang, C. Deng, D. Feng: Phys. Rev. A **51**, 73 (1995).

[33] M. Vivian, A. Kievsky, S. Rosati: Few-body Systems **18**, 25 (1995).

[34] Mukherjee et al: Phys. Rep. **231**, 201 (1993).

[35] M. Fabre de la Ripelle: Ann. Phys. **147**, 281 (1983).

[36] M. Fabre de la Ripelle: Few-Body Systems **1**, 181 (1986).

[37] W. Oehm, H. Fiedeldey, S. A. Sofianos, M. Fabre de la Repelle: Phys. Rev. C **42**, 2322 (1990).

[38] W. Oehm, H. Fiedeldey, S. A. Sofianos, M. Fabre de la Repelle: Phys. Rev. C **44**, 81 (1991).

[39] N. W. Schellingerhout, J. J. Schut, L. P. Kok: Phys. Rev. C **46**, (1992).

[40] T. K. Das, S. Roy, Pramana-J. Phys. **36**, 305 (1991).

[41] M. Fabre de la Repelle: Nucl. Phys. A **839**, (2010).

[42] M. Fabre de la Repelle: Phy. Lett. B **753**, 1 (2016).

[43] T. K. Das, R. Chattopadhyay: Fizika B **2**, 73 (1993).

[44] N. Barnea, M. Viviani: Phys. Rev. C **61**, 034003 (2000).

[45] G. J. Rampho: Phys. Rev. C **105**, 054003 (2022).

[46] G. Lacroix, C. Semay, F. Buisseret: Phys. Rev. E **86**, 026705 (2012).

[47] G. J. Rampho, L. C. Mabunda, M. Ramantswana: J. Phys.: Conf. Ser. **915**, 012005 (2017).

[48] M. Fabre de la Repelle, H. Fiedeldey, S. A.Sofianos: Phys. Rev. C **38**, 449 (1988).

[49] M. Fabre de la Ripelle, H. Fiedeldey, G. Wiechers: Ann. Phys. **138**, 275 (1982).

[50] R. M. Adam, H. Fiedeldey: J. Phys. G: Nucl. Part. Phys. **19**, 701 (1993).

[51] M. Fabre de la Ripelle: Lecture Notes in Physics **273**, 302 (1987).

[52] N. Ya. Vilenkin, G. L. Kuznetsov, Ya. R. Smorodinsky: Sov. J. Nuc1. Phys. **2**, (Ls66) 64s.

[53] J. S. Avery: Hyperspherical Harmonics: Application in Quantum Theory: Kluwer-Dordrecht (1989).

[54] M. Fabre de la Ripelle, M. I. Haftel, S. Y. Larsen: Phys. Lett. **44**, 7084 (1991).

[55] R. .M. Adam, S. A. Sofianos, H. Fiedeldey, M. Fabre de la Ripelle: J. Phys. G: Nucl. Part. Phys. **18**, 1365 (1992).

[56] R. Brizzi, M. Fabre de la Ripelle, M. Lassaut: Nucl. Phys. A **596**, 199 (1996).

[57] M. F. de la Ripelle, Y. S. Larsen: Few-Body Syst. **13**, 199 (1992).

[58] M. Hesse, D. Baye: J. Phys. B **32**, 5605 (1999).

[59] M. Vincke, D. Baye: J. Phys. B **39**, 2605 (2006)

[60] D. Baye, J. M. Sparenberg: Phys. Rev. E **82**, 056701 (2010).

[61] P. Descouvemont, C. Daniel, D Baye: Phys. Rev. C **67**, 044309 (2003).

[62] P. Descouvemont, E. M. Tursunov, D. Baye: Nucl. Phys. A **765**, 370 (2006).

[63] T. Druet, D. Baye, P. Descouvemont, J. M. Sparenberg: Nucl. Phys. A **84**, 588 (2010).

[64] G. J. Rampho: Few-Body Systems **64**, 8 (2023).

[65] I. R. Afnan, Y. C. Tang, Phys. Rev. **175**, 1337 (1968).

[66] H. Eikemeier, H. H. Hackenbroich, Z. Physik **195**, 412 (1966); Nucl. Phys. A **169**,

[67] R. E. Malfiet, J. A. Tjon: Nucl. Phys. A **127**, 161.1 (1969).

[68] G. J. Zabolitzky, K. E. Schmidt, M. H. Kalos, Phys. Rev. C **25**, 1111 (1982).

[69] G. J. Rampho: J. Phys. A: Math. Theor. 49, 295202 (2016).